



## Geoarchaeological and 3D visualisation approaches for contextualising *in-situ* fossil bearing palaeokarst in South Africa: A case study from the ~2.61 Ma Drimolen Makondo



Andy I.R. Herries <sup>a, b, \*</sup>, Ashleigh Murszewski <sup>a, c, \*\*, 1</sup>, Robyn Pickering <sup>d, e</sup>, Tom Mallett <sup>a</sup>, Renaud Joannes-Boyau <sup>f</sup>, Brian Armstrong <sup>a</sup>, Justin W. Adams <sup>g</sup>, Stephanie Baker <sup>b</sup>, Alex F. Blackwood <sup>a</sup>, Paul Penzo-Kajewski <sup>a</sup>, Peter Kappen <sup>h</sup>, AB Leece <sup>a</sup>, Jesse Martin <sup>a</sup>, Douglass Rovinsky <sup>g</sup>, Giovanni Boschian <sup>i</sup>

<sup>a</sup> Palaeoscience Labs, Department of Archaeology and History, La Trobe University, Melbourne Campus, Bundoora, 3086, VIC, Australia

<sup>b</sup> Centre for Anthropological Research, University of Johannesburg, Bunting Road Campus, Auckland Park, Gauteng, South Africa

<sup>c</sup> School of Earth, Atmosphere and Environment, Monash University, Melbourne, VIC, Australia

<sup>d</sup> Department of Geological Sciences, Human Evolution Research Institute, University of Cape Town, Western Cape, South Africa

<sup>e</sup> School of Earth Sciences, University of Melbourne, Melbourne, VIC, Australia

<sup>f</sup> Geoscience, Southern Cross University, NSW, Australia

<sup>g</sup> Centre for Human Anatomy Education, Department of Anatomy and Developmental Biology, Biomedical Discovery Institute, Monash University, Clayton, Melbourne, VIC, Australia

<sup>h</sup> The Australian Synchrotron, Clayton, Melbourne, VIC, Australia

<sup>i</sup> Department of Biology, University of Pisa, Italy

### ARTICLE INFO

#### Article history:

Received 19 May 2017

Received in revised form

10 November 2017

Accepted 4 January 2018

Available online 13 April 2018

### ABSTRACT

South Africa contains a wealth of palaeokarst deposits that have yielded hominin fossils and Early Stone Age archaeology. Despite the complex nature of deposition within many of these caves there has been a dearth of detailed geoarchaeological studies undertaken on these sites. Many sites in South Africa have been interpreted using an overly simplistic Member System based on simplified sedimentological attributes, rather than chronostratigraphic units. Many of the defined Members thus identify different, but contemporary geological processes occurring in the caves. This has caused serious confusion in reconstructing the life histories of palaeocaves and the ages of the fossil remains interred within them. It is critical to uncover new sites that have not been extensively altered by decades of data collection and destructive mining techniques employed early in their discovery. Although unmined sites present their own problems with regards to extensive colluvium cover and access to fossil-bearing units, analysing strata that is found *in-situ* enhances overall confidence of interpretations drawn. A wealth of geoarchaeological and 3D visualisation techniques can now be employed to aid in the understanding of cave life histories, as well as their excavation. In this paper we present the first attempt to integrate and publish data from a range of such methods on South African fossil bearing palaeokarst using the newly discovered Drimolen Makondo deposit as a case study. This includes the use of ground penetrating radar, 3D visualisation through photogrammetry and multi-scale 3D scanning, micromorphology and petroglyphy, palaeomagnetism, mineral magnetism, synchrotron radiation, electron spin resonance, uranium-lead dating and biochronology. Our analysis has allowed us to successfully uncover the full extent of this new ~2.61 Ma fossil bearing palaeokarst deposit and to visualise and interpret its chronostratigraphy.

© 2018 Elsevier Ltd and INQUA. All rights reserved.

\* Corresponding author. The Australian Archaeomagnetism Laboratory, Dept. Archaeology and History, La Trobe University, Melbourne Campus, Bundoora, 3086, VIC, Australia.

\*\* Corresponding author. The Australian Archaeomagnetism Laboratory, Dept. Archaeology and History, La Trobe University, Melbourne Campus, Bundoora, 3086, VIC, Australia.

E-mail addresses: [a.herries@latrobe.edu.au](mailto:a.herries@latrobe.edu.au) (A.I.R. Herries), [a.murszewski@latrobe.edu.au](mailto:a.murszewski@latrobe.edu.au) (A. Murszewski).

<sup>1</sup> indicating co-first author collaboration.

## 1. Introduction

Until the last 20 years almost everything that was known about early hominin evolution in South Africa came from a short (~3 km) stretch of the Bloubank Stream Valley in the Gauteng Province of South Africa (Bolt's Farm to Plover's Lake in Fig. 1b). The sites within the Gauteng exposures of this region are encompassed within the region formally referred to as the Fossil Hominid Sites of South Africa, colloquially termed The Cradle of Humankind (CoH) (Fig. 1a–b). The cave sites of Sterkfontein, Swartkrans and Kromdraai B have yielded the bulk of the early hominin (pre 1.0 Ma) material from South Africa. These caves all have complex multi-phase karstification histories where many phases of cave formation and infill have occurred in the same place and on the same palaeokarstic conduits. At Sterkfontein in particular the development of a more recent cave system beneath the palaeokarst has caused material to subside, collapse and be reworked into lower caverns (Stratford et al., 2012, 2014). Many of these caves within the Bloubank Valley are part of the resurgence systems for groundwater out-welling into the Bloubank; of which some may have functioned as primary resurgence caves during the early Pleistocene (Herries et al., 2010). Such caves typically have complex multi-stage karstification histories as they can function as hydrological outputs for significant periods of time, especially on static

landscapes where uplift is minimal (Latham et al., 1999, 2003).

An understanding of the Bloubank Stream Valley sites is further complicated with decades (some sites up to 80 + years) of excavation, the utilisation of various data collection methods by multiple researchers, and lastly, extensive, destructive speleothem mining in the early 20th Century (Herries et al., 2009, 2010, 2013; ; Herries and Adams, 2013). Consequently, many of the fossils recovered from these sites were ex-situ and so their location within the stratigraphy has often been assumed or reconstructed. There has also been an emphasis on how the sediments infilled the caves rather than how the caves themselves formed and evolved, which would help understand deposition within them. Moreover, when this has been attempted, due to the complexities of cave formation this was often misunderstood (Latham et al., 1999, 2003). Many sites in South Africa have been interpreted using an overly simplistic Member System based on simplified sedimentological attributes (Partridge, 1978, 1979; 2000; Bruxelles et al., 2016), rather than chronostratigraphic units. Many of the defined Members thus identify different, but contemporary geological processes occurring in the caves (Latham et al., 2003). This has caused serious confusion in reconstructing the life histories of palaeocaves and the ages of the fossil remains interned within them (Herries et al., 2009, 2013).

It is critical to uncover new sites that have not been extensively

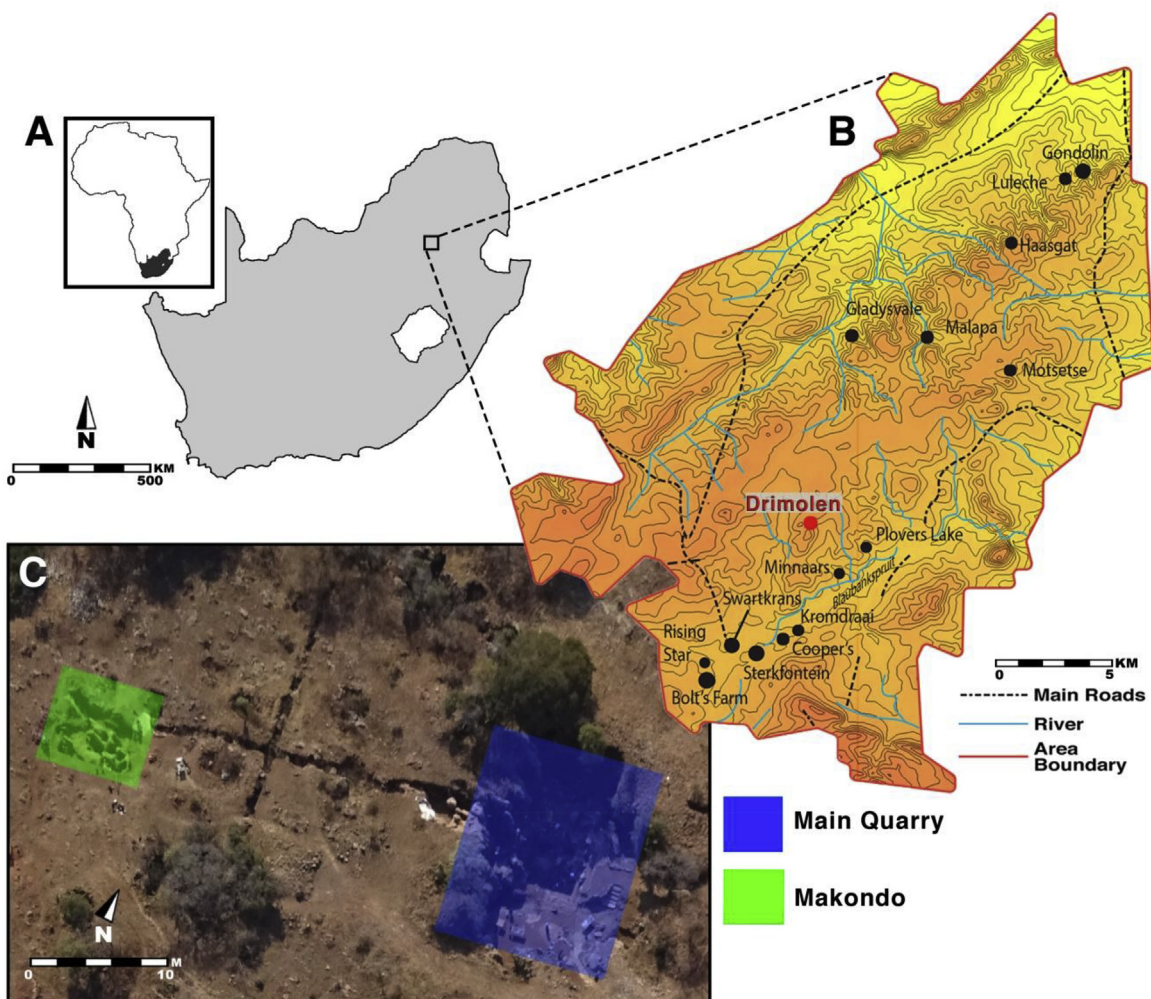


**Fig. 1.** A) The location of the Hominid Fossil Sites of South Africa UNESCO World Heritage Site (Cradle of Humankind); B) The height and location of Drimolen compared to other fossil bearing cave sites in the CoH; C) The relationship of the Drimolen Makondo to the Main Quarry.

altered by decades of data collection and destructive mining techniques employed early in their discovery (e.g. Berger et al., 2015; Dirks et al., 2017). Although unmined sites present their own problems with regards to extensive colluvium cover and access to fossil-bearing units, analysing strata that is found *in-situ* enhances overall confidence of interpretations drawn. It is not until recently with the discovery of sites such as Malapa (first discovery of the ~2 Ma *Australopithecus sediba*; Dirks et al., 2010) and Drimolen (largest collection of *Paranthropus robustus* outside of the Bloubank Stream Valley), with the only other specimen being the single tooth from Gondolin; (Menter et al., 1999; Adams et al., 2007). Therefore it is only in the 1990s and 2000s that our understanding of human evolution outside the Bloubank Stream Valley has been extended. Many of these sites, like Drimolen Cave, are water sinks from very localised watersheds that often form over very short periods of time. This is because they are abandoned for other input points due to changes in surface and groundwater flow linked to erosion (Herries et al., 2010). As such they therefore have less complex depositional histories which much less secondary cave formation.

To date, the discovery of new hominin sites has continued to rely on the identification of 20th Century speleothem mining activities and related breccia dumps, as at Malapa, Haasgat and Drimolen Main Quarry (Dirks et al., 2010; Herries et al., 2014; Leece et al., 2016). At some of the classic sites, hominin remains would never have been found if it were not for the early exploitation of speleothem mining. At sites such as the Makapansgat Limeworks and Drimolen Main Quarry, mining has in some ways aided palaeoanthropological research in the establishment of the depositional sequencing throughout the cave (Latham et al., 1999, 2003; Herries et al., 2013, 2017). In most other cases, mining activities have significantly obscured stratigraphic relationships, where the correlation of hominin fossils within dump sites to their associated stratigraphic position is impossible to establish (Herries and Adams, 2013). The vast majority of sites that have been extensively mined have mostly been identified and explored, especially with the advent of Google Earth. However, new fossil sites still exist in the region that have never been mined for speleothem, mainly because the speleothem layers that exist within palaeocaves do not occur at the surface, or are of poor quality (impure) for making lime. Or the fossils occur in a completely different cave context as with *Homo naledi* at Rising Star (Dirks et al., 2017). The fossils from these sites are therefore *in-situ*, with the only disturbance of sediments being during secondary karst processes, such as the formation of makondokarren (a karst pavement of solution pockets within the dolomite formed under colluvial cover) or more recent caves (Brink and Partridge, 1980; Herries and Shaw, 2011; Herries et al., 2017). Moreover, several newly discovered sites, such as Malapa and Brad Pit at Bolt's Farm have only been disturbed by speleothem mining in a minimal way (Dirks et al., 2010; Gommery et al., 2012). Such undisturbed, or minimally disturbed sites, present their own challenges with regards excavation and geological analysis.

One such minimally disturbed site is the newly discovered Drimolen Makondo palaeocave deposits (Rovinsky et al., 2015). The remanent palaeocave deposits were only minimally exposed by mining and other karst processes (Figs. 2–3). Thus, while the fossil bearing breccia is only around 50 m from the hominin bearing Drimolen Main Quarry deposits, and while it had been previously noted, it was never excavated or sampled until 2014. Here we describe our geoarchaeological approach for the study of such minimally mined sites using a variety of techniques that are either novel or atypical with regards their use in these types of sites. However, they are presented as a package of broad geoarchaeological techniques that have never previously been used in the region. Our aim is to both show the effectiveness and challenges of using these techniques on such complex sites and to show the

range of applications that are incorporated in a modern geoarchaeological study of fossil contexts. This has enabled us to establish a preliminary chronostratigraphic framework for the site and to understand the fossil distributions that occur in the site, thus allowing us to effectively target future excavations.

### 1.1. Site setting

#### 1.1.1. Regional geological context

The regional contexts of palaeocave sites is critically important when attempting to understand the placement and abundance of palaeokarst within the CoH. Drimolen is located at a high point in the Gauteng Malmani dolomite (GMD) landscape at ~1543–37 m above mean sea level (amsl) (Fig. 1b) and NE of sites such as Sterkfontein, Swartkrans, Coopers and Kromdraai. Drimolen is closest to the fossil site of Plover's Lake, located in the eastern end of the Bloubank Stream Valley ~2.3 km to the SE of Drimolen at 1446 m amsl (de Ruiter et al., 2008) (Fig. 1b). Uniquely, Drimolen does not lie in an extensive river channel today and occurs close to the top of a hill with an elevation of 1588 m amsl, and one of the highest points in the Gauteng Malmani Dolomite. Clues as to why Drimolen is located in this rather unique location, with few other recognised fossil sites close to it, can be found in structural and petrological attributes in the regional geology. This has instigated a series of regional geological and structural mapping projects at Drimolen, as well as other sites of higher altitude outside of the Bloubank Stream Valley.

These analyses are still within their preliminary stages, however current data from studies at Drimolen show multiple large igneous intrusives found on the surface, alongside dolomite and chert outcrops. Detailed knowledge of regional features like this are important when attempting to ascertain mode of formation. This is because factors that influence karstification are not only reliant on the solubility of the rock type (high solubility rocks typically include limestone, dolomite and gypsum), but are also characterised by secondary fracture porosity and structure location. As the emplacement of these intrusive bodies would have resulted in extensive deformation, geological markers are likely key to the evolution of the karstic landscape at these high altitudes. Lastly, as these subvolcanic intrusions are much more extensive at depth, this also may explain the elevation of the dolomite in this part of the GMD. These studies will ultimately enhance our knowledge about the material located within palaeokarst deposits, but also better our ability to locate untouched, *in-situ* palaeokarsts within the dolomitic landscape.

#### 1.1.2. Site history and excavations

The hominin bearing palaeocave system of Drimolen (Fig. 1b) was first discovered in the 1990s (Keyser et al., 2000) and has since yielded numerous fossils of *Paranthropus robustus*, including the most complete *P. robustus* skull yet found (DNH 7) (Keyser, 2000; Keyser et al., 2000), as well as early *Homo* and a range of other mammals (Moggi-Cecchi et al., 2010; Adams et al., 2016). The site has also produced the largest collection of purported bone tools from any of the Plio-Pleistocene early hominin bearing sites with over 100 potential tools currently known; although to date only a small proportion have been fully studied (Backwell and d'Errico, 2008). All this material originates from the Drimolen Main Quarry (DMQ) (Fig. 1c) where lime miners concentrated their efforts in extracting speleothem from the palaeocave system in the early 20th Century; opening exposure of the site to its current form. The mining collapsed part of the breccia deposit into smaller blocks, although the DNH 7 (aka Eurydice) block remains mostly intact. Due to burial, and the smaller size of the breccia blocks, decalcification of the deposits was intensified over the last ~100

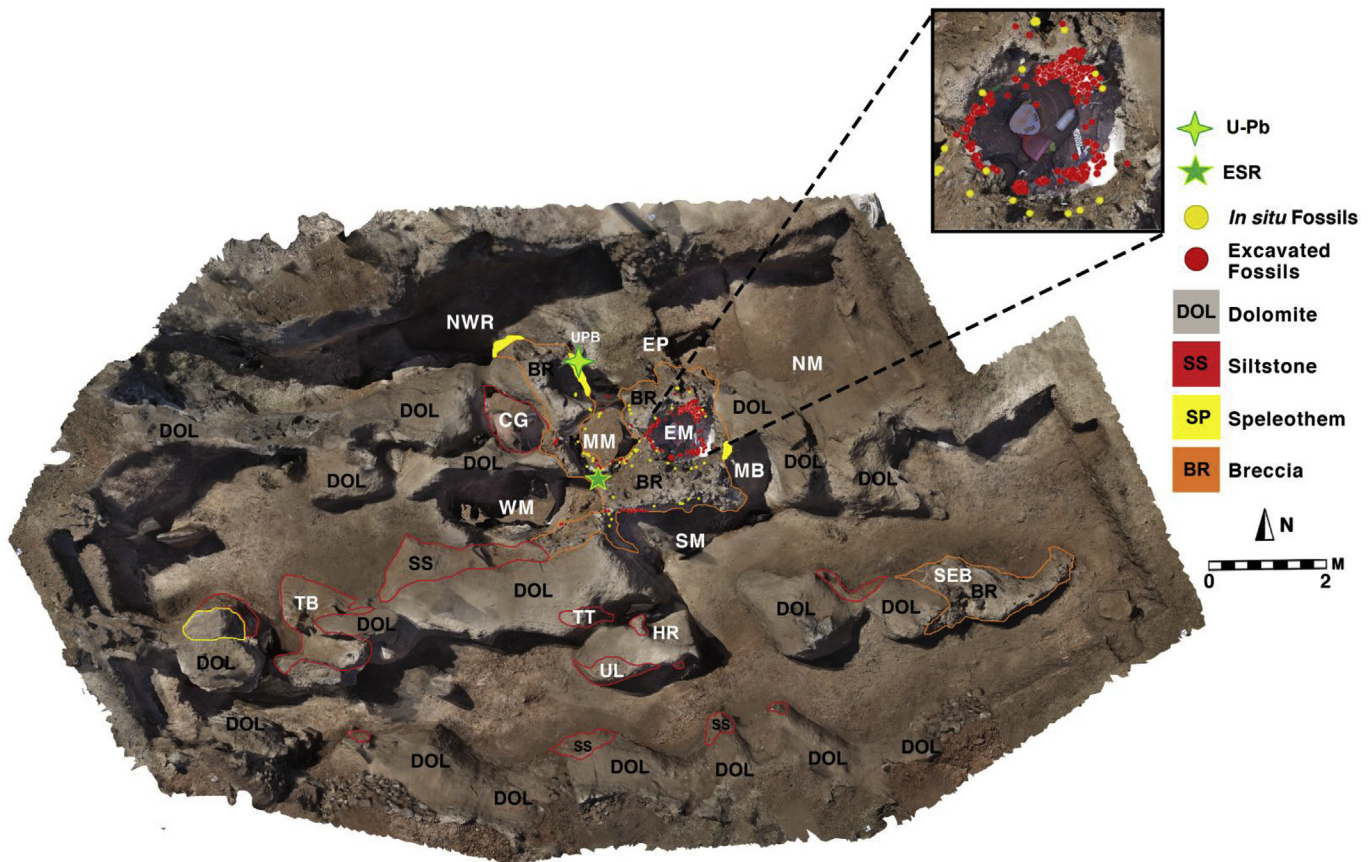


**Fig. 2.** Photogrammetry model of the Drimolen Makondo at the end of the 2016 excavation season. The sedimentological nature of the outcrops is shown as well as piece plotted locations of in-situ and excavated fossils that are concentrated in the central breccia. The methodology for creating the photogrammetry model is outlined in Armstrong et al. (2018). The named features of the site are also shown (MM = Main Makondo; EM = Eastern Makondo; WM = Western Makondo; NM = Northern Makondo; SM = Southern Makondo; NWR = North West Rift; MB = Maddie's Bath; CG = Chris' Gym; TB = Traynorberg; TT = The Tongue; THR = The Hanging Remnant; UL = Uluru; SEB = South East Breccia).

years since this occurred. However, because decalcification has been so recent much of the fossil material is extremely well preserved despite not being encased in breccia. These decalcified collapse deposits around the DNH 7 block have been the main focus of the excavations to date.

A long trench (referred to as 'Keyser's Trench'), was also excavated in the 1990's which extended west of DMQ for approximately 50 m to a small round solutional tube, known locally as a makondo (Brink and Partridge, 1980). This makondo has been shown to be richly fossil bearing and is now termed the Drimolen Makondo (DMK; Fig. 1c). Only a small layer of basal speleothem occurs in this deposit (Fig. 5), so unlike DMQ, DMK was not extensively mined for speleothem. This makondo feature is dissolved into fossil rich indurated palaeocave sediments. Despite the density of the fossils DMK has not been previously studied because only a very small portion of the palaeocave deposit was exposed. However, a study of the makondo feature (now known as the Main Makondo; DMK-MM; Fig. 2) in 2013 identified a significant portion of loose and densely fossiliferous sediments adhering to its wall and in threat of collapse. A rescue excavation was undertaken to remove this material, which forms the basis of the fossil material described by Rovinsky et al. (2015). This densely fossiliferous material contained articulated partial bovid feet, as well as carnivore and suid remains and included taxa previously unknown in the Drimolen Main Quarry (Keyser et al., 2000; Rovinsky et al., 2015; Adams et al., 2016; also see below). It was determined from the excavation that the sediments represented decalcified breccia, rather than

more recent makondo in-fill, because articulated fossil remains within the loose sediments continued into the solid breccia. North of DMK-MM is a SE to NW trending solution feature partly mined, termed here the North-West Rift (DMK-NWR) (Fig. 2). This feature exposed further palaeocave sediments on its western and southern walls and this formed the known extent of the site at the end of 2013.

Extensive excavations of DMK began in 2014. Stripping of colluvium from around the exposed fossil bearing exposures was guided by ground penetrating radar analysis (GPR: see next section). Excavations were conducted with a Topcon<sup>®</sup> GPT7500 reflectorless Total Station Theodolite (TST), with all fossils and stratigraphic information piece-plotted and digitally recorded. Excavation data were also recorded on an iPad<sup>®</sup> using the Tap-Forms<sup>®</sup> application. Colluvium removed to the east of the DMK-MM identified a second makondo feature infilled with the same palaeocave deposits, subsequently termed the Eastern Makondo (DMK-EM). This has been the most fossiliferous part of the site (Figs. 2 and 3a) mainly because it has been dissolved into the central breccia deposit of the DMK. Stripping of colluvium to the South of DMK-MM in 2014 revealed a southern wall of this Central Breccia (DMK-SM). This has been shown to be extensively fossiliferous throughout the 2015 and 2016 excavations. Throughout 2015, 2016, colluvial cover was removed from extensive areas to the west, south and east of the Central Breccia as well as the excavation of the WM, which was identified by GPR analysis. The DM-CG Makondo feature was also excavated, although it yielded few fossils because

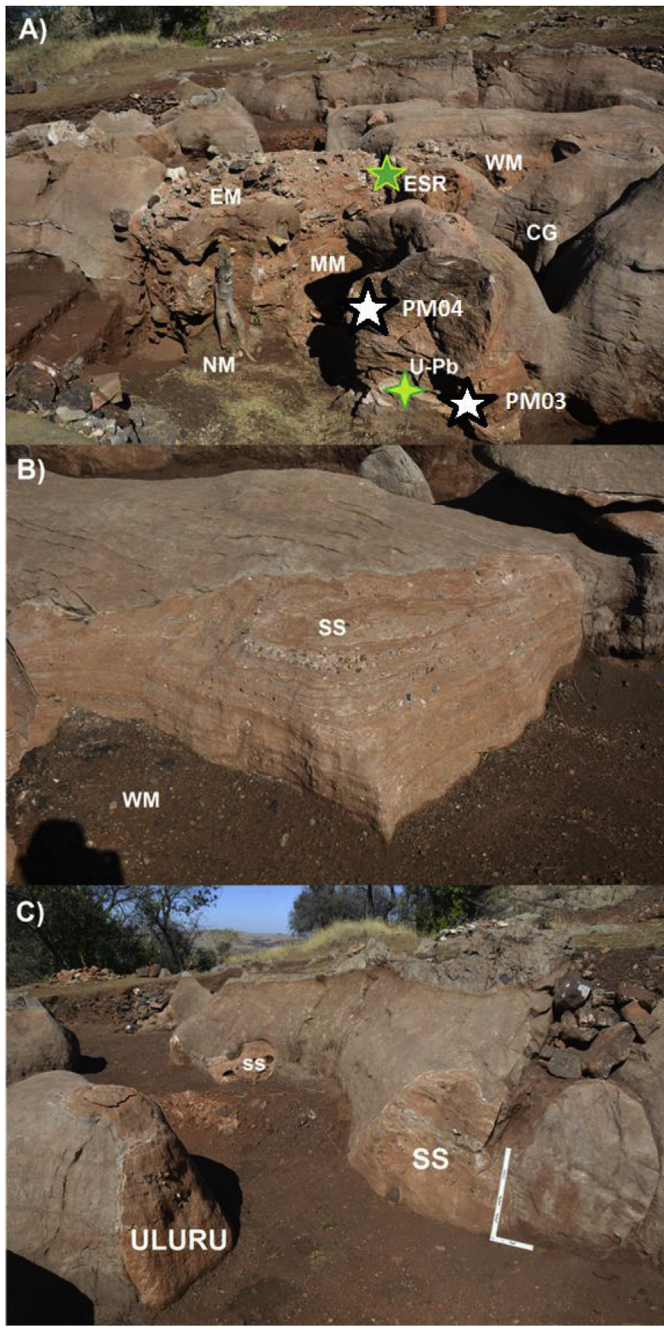


**Fig. 3.** A) Looking south from the Northern Makondo across the Central Breccia of DMK and showing the location of the ESR and U-Pb samples, as well as the various other Makondo features. B) Example of well laminated siltstone and sandstone on the southern side of the Western Makondo. C) The various small remnants of siltstone and sandstone along the southern dolomite wall of the excavation area.

it is dissolved into siltstone deposits that are generally macrofossil poor. This is due to the low energy winnowing events that deposited it and its deposition in a distal part of the cave away from the entrance. Presumably this part of the cave was simply not used by animals accessing other parts of the cave or the cave was inaccessible to them (Fig. 3b). Similar remnants of well laminated siltstone and sandstone deposits were uncovered stretching to the SW of the Central Breccia (DMK-TB; Figs. 2 and 3c), in small areas around DMK-UL, TT, HR and along the southern wall of dolomite where they occur as very small remnant patches. The formation of

makondokarren has extensively dissolved away the former palaeocaves sediments, especially the siltstone and sandstone deposits. This is quite common as the calcite formed within and indurating the palaeocave deposits is purer and more easily dissolved than the dolomite itself. It is also very common in the region for more recent caves to form within or at the interface of palaeokarst (Herries et al., 2010). Removal of colluvium to the SE of the Central Breccia revealed another small area of breccia, but it was not densely fossiliferous, likely representing the base of the talus cone that formed prior to the Central Breccia. While the excavation of DMK-EM has yielded extensive fossil remains (including those partly solidified in the wall still) that show the sediments within the makondo consist of decalcified breccia, other makondo features like WM consist of later colluvial fill and contained no fossils, except at the very edge of the makondo features where they are actively being dissolved out of the siltstone and breccia. This is characteristic across the site where fossils are only found close to the breccia and siltstone and sandstone walls of the makondos (Fig. 2). Fossils likely once occurred in the central portion of the makondos but have since been dissolved away. The following describes our unique methodology and preliminary results for attempting to establish both the extent of these deposits, their stratigraphy and age over the last 4 years.

## 2. Subsurface exploration and site visualisation

One of the fundamental differences in assessing extensively mined vs. *in-situ* deposits, is the equipment necessary for locating and recording minimally exposed palaeocaves. Initial research at DMK was greatly enhanced through early GPR analysis, which provided useful information that eased safety concerns and ultimately aided the efficiency and productivity of the ensuing excavations. Subsequent 3D modelling in the forms of laser scanning and photogrammetry, have also provided useful visual tools aiding in successive laboratory work and teaching.

### 2.1. Ground penetrating radar analysis

Ground Penetrating Radar (GPR) technology is frequently used in karst landscapes as a geotechnical tool for the detection of sinkholes and to aid in the assessment of geological stability for mine sites and for safety assessment of land developments (Benson, 1995; Chalikakis et al., 2011; Neal, 2004; Rodriguez et al., 2014). Its use in detecting caves, cavities and dolines and assessing archaeological deposits has been well established in other parts of the world, including the U.K (Chamberlain et al., 2000), Spain (Pueyo Anchuela et al., 2010) Slovenia (Gosar, 2012) and Brazil (Reis et al., 2014). Such assessments on South African palaeocaves have never been attempted, therefore, this study represents the first of its kind on deposits of this type.

Primarily the aim was to assess the extent and characterise the form of the DMK deposits to assist in the excavation process and to aid in the interpretation of the cave system. To this end a number of GPR surveys were conducted using a range of GPR antennae. The first survey in 2014 prior to excavation, was conducted on a 13 m E-W grid with survey runs spaced every 0.5 m N-S (Fig. 4). The survey utilised a MALA<sup>®</sup> Pro Ex GPR system with a 500 MHz shielded antenna, with data processing conducted in both Mala Object Mapper<sup>™</sup> and GPR Slice v7.0<sup>®</sup>. Initial results indicated that the 500 MHz survey proved to have excellent resolutions between the depths of 0.5 m-4m. (Fig. 4). These data suggested that more makondo features occurred beneath the hillside colluvium and that in a couple of cases large voids were also identified (Fig. 4). Digging at the base of the Main Makondo in 2014 allowed access into one of these void features (the West Makondo; DMK-WM; Fig. 2), containing further

articulated fossil remains in its walls including an articulated primate leg. The covering colluvium of DMK-WM was later removed in 2015 to reveal the full extent of the ~3 m deep solution tube.

In addition to voids, banded linear features were identified within the radargrams (Fig. 4), and these were found to correspond with the surface outcropping of the chert within the dolomite; a common feature in the Malmani dolomite succession. This enabled assessment of the dip and angle of projection of the chert, where we postulate that the roof of the makondo cave would have formed along this more durable rocktype; as is the case for a cave system located underneath the southern end of the DMK (Porcupine Cave). The GPR thus limited our need to strip colluvium off large areas of the hillside, target specific features for subsequent excavation and

provided initial interpretations of the morphology and formational characteristics of the solution cavities. This tool also provided an important safety feature in that we are able to identify buried makondo features that could collapse in when having the overburden colluvium removed during periods of excavation.

## 2.2. 3D modelling

Traditionally the stratigraphy of South African hominin bearing caves sites has been documented by either a series of two dimensional sections tied to a map of the site with the aim of recording a series of sections to highlight lateral variation (e.g., Brain, 1958; Keyser and Martini, 1991; Latham et al., 2003), or by the use of a

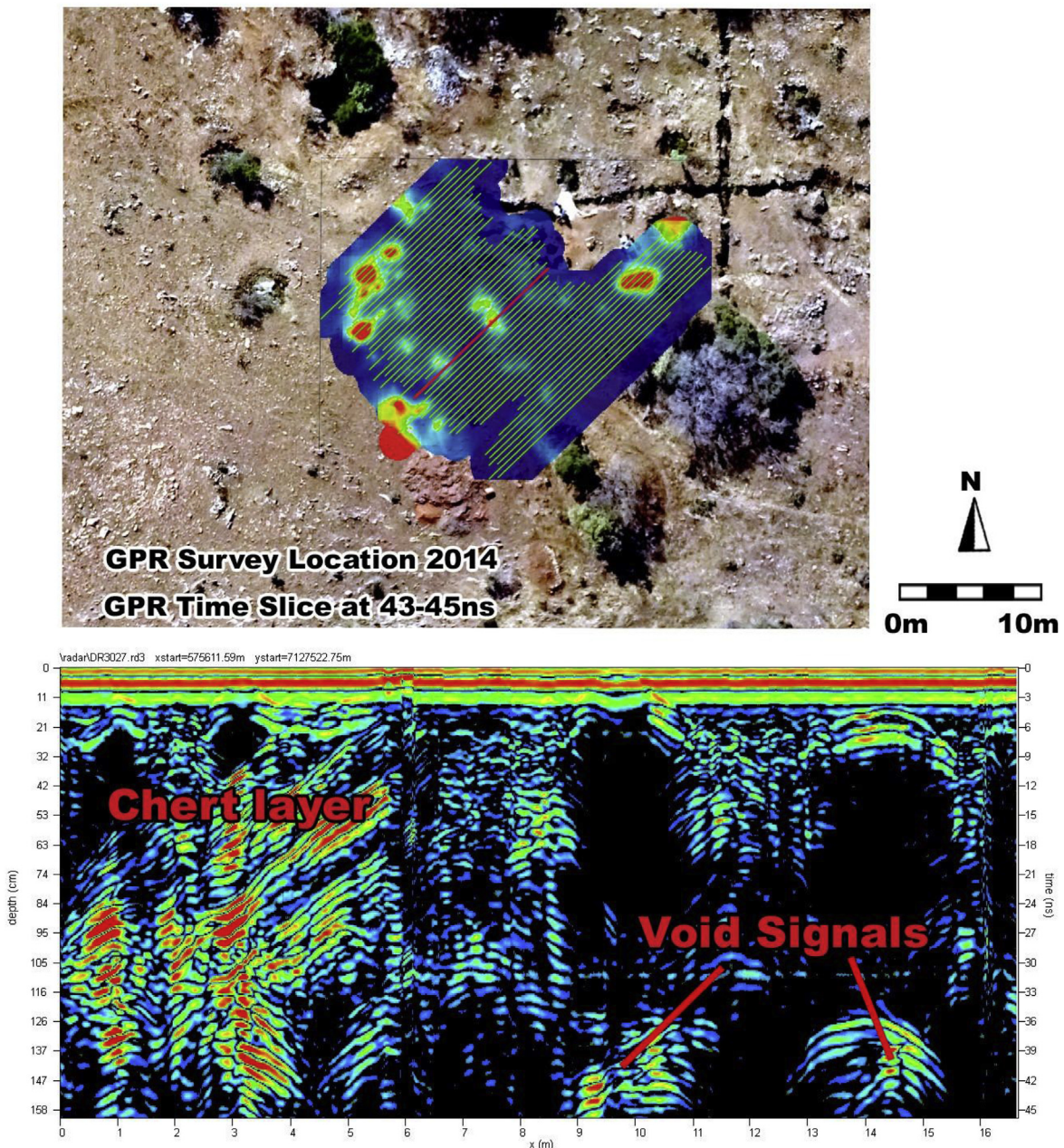


**Fig. 4.** GPR survey undertaken around the Drimolen Makondo using a Mala® GPR ProEX System with a 500 Mhz antenna. Typically, high-resolution imagery was produced between the depths of 1.5 m-3m, although due to surface outcropping dolomite, and uneven ground surfaces some radargrams show patches of off ground signals. Electrical contrasts are high between air filled solution pockets and the surrounding dolomite, as a result these can be seen very clearly on the radargram. The chert bedding to the southwest of the site that likely formed the former roof of the cave clearly shows up on the left hand side of the radargram.

simple composite sections of stratigraphy that are amalgamated from different parts of the sequence to create a virtual chronostratigraphy (Partridge, 1978, 1979; Herries et al., 2006a; b; Stratford et al., 2012). In an attempt to fully document the complex nature of the site and the deposits, and to supplement the Total Station location recording of samples and fossils, two methods of 3D modelling were tested to assess their suitability for this environment (Armstrong et al., 2018). Photogrammetry and laser scanning were applied at various stages of the excavation process between 2015 and 2016, with two versions of models generated at the start and end of excavation seasons (Fig. 2). The photogrammetry surveys were conducted using a Nikon D80 (AF-S DX Nikkor 35 mm f/1.8G fixed lens; Nikon Corp., Japan), and processed with Agisoft PhotoScan (Ver. 1.1.6). Depending upon the size of the area to be captured, between 500 and 1000 photos were taken for each excavation phase using the method outlined in the Agisoft user's manual (Agisoft, 2013). Processing was conducted on a 6 core Intel i7 CPU with a Nvidia GTX 780 GPU and 48 GB of RAM, and the resulting model was orthorectified onto the Drimolen palaeocave grid using Agisoft ground markers that were recorded using the TST. Outputs were generated in \*.las point cloud format and a colourised textured \*.wrl 3D model format compatible with ArcScene (ESRI). Both the site TST data and the 3D models are visualised using ArcScene 10.3.

Subsequent models were generated with an MS50 Leica Multi Station with laser scanning function. The MS50 has the ability to operate as a TST, allowing scans to be conducted and automatically georectified using the site grid. Depending upon the excavation phase a number of scan setups were needed, taking between 5 and 10 to capture each makondo scene. The scan station setups were typically located between 3 and 5 m from the edge of the excavation and optimum scan settings were set at 5 mm resolutions. A discreet zone around the excavation was outlined using the inbuilt software in order to capture the site extent and provide a dense overlapping point cloud. The inbuilt camera of the MS50 was not used due to high glare field conditions and as a result only greyscale point clouds and models were produced. The automatically georectified point cloud data was exported as \*.las or \*.e57 files using Leica Infinity software (Leica Geosystems), and imported into 3DReshaper to generate 3D models in VRML (Virtual Reality Markup Language) format. These models and the associated point clouds in \*.las format were again imported into the ArcScene and provide additional high resolution, highly accurate models for the project. By effectively visualizing the different deposits, and recording the 3D location of the fossils, the process of identifying which sediments relate to the original cave system and which represent later infill processes can be determined to a greater level of accuracy.

### 2.3. Structured light section scans

While photogrammetry is ideal for scanning open air palaeocave remnants like DMK, and dark portions can be scanned using a 3D scanning multistation (Armstrong et al., 2018), these methods both struggle, or are impossible within the narrow, deep makondo features. This can be seen where there are blank portions at the base of the makondo features (Fig. 2). This can be overcome by the use of other 3D scanning options such as the ZEB1 handheld scanner, although this does not create a full photorealistic model like photogrammetry. Because of this, we instead used an Artec Space Spider structured light scanner that can capture high resolution true colour image scans. This scanner (or the Artec Eva medium object scanner) can be used to both fill in hard to reach areas of the site 3D model, to scan fossils still encased in breccia in high resolution, or to scan sections before and after sampling

(Fig. 5). In particular, the Artec Space Spider Scanner's small size ( $190 \times 140 \times 130$  mm), light weight (0.85 kg), and ability to operate from a portable battery pack mean that it is ideal for use in confined and/or hard to reach spaces. Additionally, the manufacturer stated specifications combine a .05 mm point accuracy with the capacity to generate up to a 0.1 mm final object resolution. For these reasons, the scanner has also been used to scan fossil clusters during excavation, as well as the fossils themselves once extracted.

The combination of a photo – real texture and an extremely accurate three-dimensional polygon means that post-processed scans, despite being captured in the field prior to excavation, are sufficiently accurate as to allow fine-grained assessment of morphology (in the case of fossil specimens) or stratigraphy (in the case of geological features). The figures presented here were captured using an Artec Space Spider Scanner capturing 7.5 frames per second, powered by the manufacturer supplied portable battery pack. Post-processing was undertaken using Artec Studio 11, following a workflow adapted from that suggested by the manufacturer. The large size of the raw scans (up to 5gbs per scan for 6 separate scans) and the resultant amount of time taken to post-process these scans in Artec Studio 11, was the principal limiting factor for this method. More specifically, highly accurate scans mean larger scan file sizes, and despite operating an Acer Predator gaming laptop with a Nvidia graphics card and 16gb ram, post-processing times for each object ran as long as 10 h. Thus, while in principle there is no upper limit to the size of the objects that could be scanned using the highly accurate Artec Space Spider Scanner, the processing power of commercially available laptops provide a practical limit. Thus, we consider that the size of the scans that we have presented here approach the upper limit for the size of objects that can be efficiently captured and post-processed using the Artec Space Spider Scanner in a fieldwork setting.

### 3. Stratigraphy and sedimentology

Drimolen Makondo contains multiple solution cavities

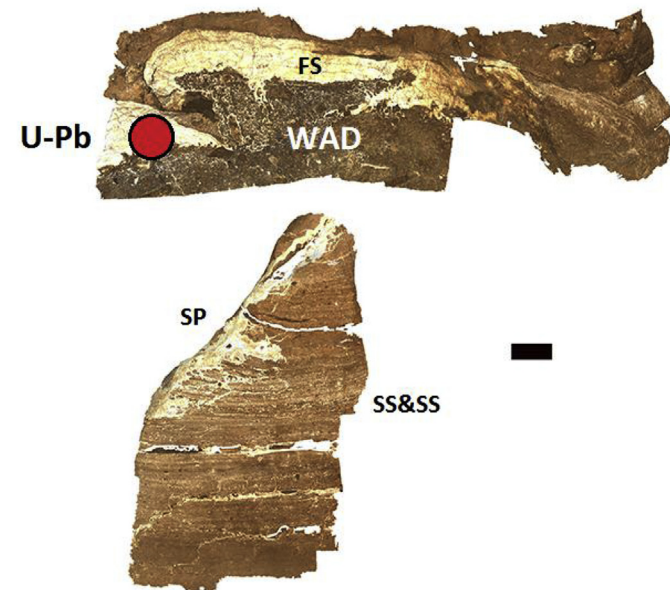


**Fig. 5.** Artec Space Spider 3D surface Scans of Upper: U-Pb dated (~2.664 Ma) basal primary flowstone (FS) overlying WAD in DMK-NWR and then overlain by siltstone and sandstone deposits (PM03); Lower: Well laminated siltstone and sandstone (SS&SS) deposits from the very back (west) of the cavity, showing secondary intrusive flowstone speleothem.

(commonly referred to as makondos) that have been infilled by decalcified breccia and soil (Figs. 2 and 3). Features similar to this have been identified throughout the Vaal River (Partridge and Brink, 1967) and in hominin bearing South African palaeokarsts (Brink and Partridge, 1980). The nonindurated sediment within the site, as well as the solution cavities (or makondos) themselves, are formed through decalcification of the surrounding breccia (Rovinsky et al., 2015). Specifically, where the acidity of the soil is heightened by deep rooted vegetation, burrowing activity and fluid filtration through cracks and joints in the rock. However, this is not the case in all the makondos at DMK, as more recent cave forming processes can drain these makondos due to collapse or fluvial regimes. In such cases, they are often refilled with more recent colluvium. It is important to identify which processes have formed each deposit, as the former will contain fossils contemporary with the palaeokarst, whereas the other will contain younger intrusive fossils. This is critical to determine, as temporal mixing of younger and older sediments has been noted at other palaeocave sites in the region and can lead to misinterpretations about the chronostratigraphical history of the site (Blackwell, 1994; de Ruiter, 2003; Reynolds et al., 2007; Herries and Adams, 2013).

To assess these fundamental questions about the depositional processes of the site, we first use basic geological principles of superposition and fundamental concepts of karst processes to present a preliminary interpretation of the stratigraphy. The various deposits formed within the closed cave system and during infilling stages, are represented well within the various stratigraphic sections of the DMK palaeocave. Hence, this site presents a favourable case study for various sedimentological and micromorphological analyses. At the contact with the basal dolomite at the western wall of the DMK-NWR, dark grey, manganese-rich residue (wad; Fig. 5) has formed through the dissolution of the dolomite. This formation along with the overlying NW-SE dipping flowstone unit (~15 cm thick) likely formed in a closed environment, before the cave system became exposed to the surface. Large blocks of dolomite and chert stratigraphically above the flowstone are evidence of roof collapse (Figs. 3a and 6). On the northern wall of DMK-MM this unit contains a massive fallen dolomite block (around 1 m long). Although not as densely populated with fossil remains as the units above, this unit does contain few identifiable fossil specimens, including a bovid horncore.

This basal talus cone layer is overlain by dense, fossil-rich breccias with interbedded siltstone and sandstone units. In some areas of the DMK this unit directly overlies the basal flowstone discussed above. The contact between these is sharp and suggests a hiatus of some duration. This deposit contains a large number of isolated fossils as well as semi-articulated element sets that tend to be concentrated within particular horizons. Many have seemingly been crushed by the deposition of later deposits. The long bones are generally well preserved and lie parallel to the bedding planes, whereas the pneumatised ones and the crania are crushed and collapsed *in-situ*. The uppermost finer clastic units (namely siltstones and sandstones) are rich in semi-articulated and unarticulated micromammalian remains and represent the infill of the entire eastern portion of the cave, which represents the rear of the cave where fine grained material has been winnowed from the clast supported breccias that occur on the eastern side of the site, near to the original entrance (Fig. 3b and c, 5). The most representative form of all these units is located in DMK-MM (Figs. 2, 3a and 6) and has been used as a reference point for the macrofossil bearing depositional profile of the site. We do not extensively describe all the sections at the site in terms of their sedimentological components because this is ongoing work and DMK is also simplistic enough in its deposition in the vast majority of the deposition at the site consist of a single phase of deposition with simple lateral

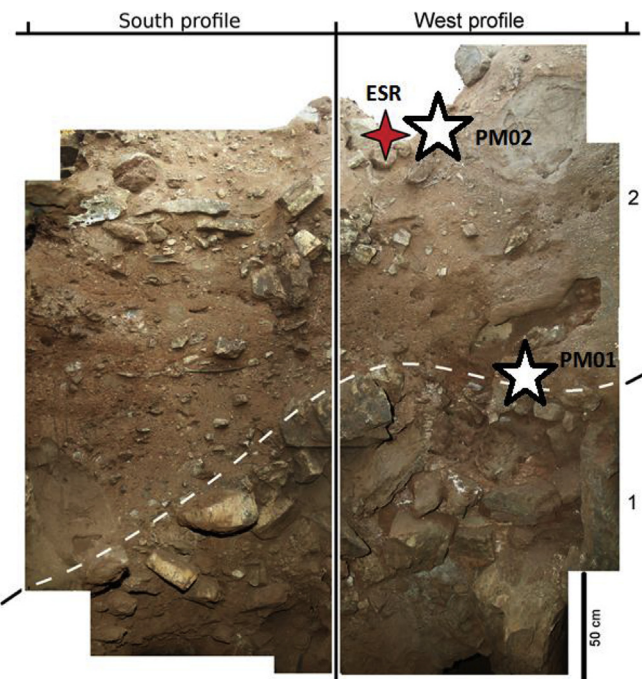


**Fig. 6.** DMK Main Makondo photomosaics of west and south profiles. 1: slightly cemented coarse dolomite and chert rubble, with red earth matrix. 2: strongly cemented and bone-rich siltstone/sandstone, with chert and dolomite clasts. Location of US-ESR date discussed in section 5.3. shown. (For interpretation of the references to colour in this figure legend, the reader is referred to the Web version of this article.)

variation of clast sizes related to their location from the original entrance (this is further confirmed by the geochronology below). This interpretation presents a good basis before completing micromorphological analyses (see 4.1.), which is used to conceptualise a more comprehensive profile at DMK, with a greater understanding of site-specific formation processes (see 4.2.).

### 3.1. Micro-scale analysis

Sediment micromorphology is a powerful technique used commonly in geoarchaeology, that provides in-depth perspectives about soil and sediment formation and evolution. Common applications in both open air and cave sites, include identifying temporal occupational intensities, sediment type, post-depositional disturbance, cultural modification of the sediments and stratigraphic correlations. While its use is well-established in several research contexts worldwide (Davidson et al., 1992; Karkanas and Goldberg, 2007, and reference therein), African Pliocene and early Pleistocene palaeoanthropology is still not extensively using this technique to help inform them about cave formation processes and taphonomy. The integration of micromorphology with advanced stratigraphic techniques, like depositional modelling, is the key to understanding the real stratigraphic relationships between sedimentary bodies and consequently to building a robust chronology and context for the fossils.

Explorative micromorphological observations (see Stoops, 2003 for methodology and terminology) were carried out on multiple thin sections, extracted from the finer silty sandstone unit, the underlying coarser brecciated material as well as the basal wad in the (DMK-NWR; Figs. 3 and 5). Portions of each unit were extracted from the samples collected for resin impregnation, where the rest of each sample was kept for potential geochemical or sedimentological analyses. Once resin was set, thin sections were cut (~30 µm)

for micromorphological analysis. Detailed steps of impregnation and subsequent thin sectioning were replicated from Fitzpatrick (1984). Each of these slides were assessed under a polarising petrographic microscope, which is most useful for identifying geological and geomorphological attributes under plane polarising light (PPL) and cross polarisation (XP). Features that were of primary focus for karst geomorphology includes the optical properties of minerals, fluvial petrology; specifically, structural features related to grain deposition and transport medium; and lastly, identification of cementing material that fills pore spaces during diagenesis.

Finer microstructure generally characterises the stratigraphically higher siltstones and sandstone (Fig. 7a), whereas underlying microstructure of breccia samples is somewhat coarser. However, thin (1–3 mm-thick) layers of coarser and finer material are common throughout both units. The related distribution pattern is generally coarse monic within the coarser layers. These coarser units appear better sorted and were likely transported from the finer microstratigraphic units (Fig. 7b). The basic mineral fraction is composed of silt-to very coarse sand-size angular to subangular grains, mostly of mono- or polycrystalline quartz. Fine white mica flakes are also frequent.

Courser samples are typically sub-angular to angular clasts, greatly varying in size range from pebbles to silts. However, most particles typically exist within the sand fraction. Traces of alteration occur on mineral grains, mostly as coatings of pedogenic iron/manganese-oxide, or as infillings within cracks (Fig. 7b). Common rounded aggregates (pedorelics) of fine material are common throughout silt-sandstones; these are amorphous and stained by iron oxides or preserve traces of stipple-speckled b-fabric, and include silt-size quartz crystal. The distinctive rust colour of ferric iron oxides seen throughout these slides is further evidence for chemical weathering of iron oxide minerals from banded iron. In this case goethite and haematite are most common. Small fragments and aggregates of vegetal organic matter stained by Fe/Mn oxides are also relatively frequent some samples. Lastly, tiny bone flakes and splinters, as well as microfauna remains are also common throughout (Figs. 7c and 8). All layers are thoroughly cemented by sparitic calcite; large anhedral crystals (Fig. 7b) with semi-frequent triple points; here, the calcite is often dirty, with dark amorphous inclusions.

### 3.2. Site formation processes

Silicate and karst weathering as well as the alteration of carbonates all provide sources of Mn<sup>2+</sup> to surface and ground waters, especially since Mn<sup>2+</sup> is highly soluble (Johnson et al., 2016; Turekian and Wedepohl, 1961). This presence of Mn<sup>2+</sup> irons also formed the preferential precipitation of wad present at the base of the eastern exposure of the North-West Makondo (Figure 3, 5). Preliminary analysis of the overlying flowstone, exposed in the DMK-NWR indicates that it was formed in a closed environment, i.e. when the cave was still predominantly closed, as it contains virtually no detrital material. The position of the entrance when the cave opened, can be inferred from the distribution of the dolomite and the spatial organisation of the large rubble clasts. From this we approximate the initial opening was probably located in an area to the east of the current exposures.

Relative particle size distributions differed through the stratigraphical profile at DMK, where lateral variation in size and sorting of grains indicates discrete periods of heightened energy transportation during deposition. The siltstone/sandstone units derived from several phases of cave partial flooding, with variable flow energy indicated by sequences of finely layered coarse/fine sandstone/siltstone layers. Fine material was subsequently washed from

coarser grain-size sediments by decreasing-energy flow regimes. Short-distance transport is suggested also by the macrofauna bone remains, which are generally well-preserved and sometimes semi- or completely articulated. It is also likely that (parts of) carcasses were deposited into this part of the cave during phases of flooding or by carnivore denning activity, although the low number of complete macrofaunal remains in the siltstones and sandstones may indicate that the latter was perhaps not a primary mechanism for deposition. It is also noted here that the abundance of clays throughout the stratigraphic profile may also be a product of deposition during slow fluid filtration into the karst. Another explanation for this, is intense weathering caused by prolonged sub-arial exposure of sediments. Due to the age of these sediments, prolonged exposure and subsequent weathering is likely a more probable cause.

Interlocking crystals or a mosaic of sparite (sparry calcite) cement is the primary infill within void spaces of samples throughout DMK and is crystallised during diagenesis as pore spaces are filled relative to the groundwater level. The supersaturation of calcite ( $\text{CaCO}_3$ ) within water is also clear from the abundance of well-defined flowstone precipitation, where this source of calcium carbonate originates from the dissolution of the surrounding host rock (dolomite;  $\text{CaMg}(\text{CO}_3)_2$ ). This environment, with the added presence of Mg<sup>2+</sup> ions also formed the preferential precipitation of aragonite in some cases (Martini and Kavalieris, 1976), visible in samples within the breccia and within the basal flowstone (Fig. 12). Understanding such processes is critical for evaluating both site formation but also that geochronological methods are dating primary and non-diagenetic features. For example, in the case of speleothem that it is deposited with the fossil bearing sediments and that it is not a remnant false floor that is older than the deposits beneath it, or a secondary infill that is much younger (Fig. 5). In the case of palaeomagnetism, that the magnetic remanence was locked into the sediments early on in the history of their deposition and that subsequent processes have not remagnetised the deposits.

### 4. Faunal remains and biochronology

Palaeocave faunal assemblages provide useful datasets to aid in developing ecological and environmental reconstructions. In addition, once temporally distinctive palaeontological events have been established; such as the occurrence of a temporally limited species or genus, stratigraphically based biochronological data becomes useful to assess age relationships of fossils and associated units in which they are imbedded. In turn, the more emphasis that is placed on faunal analysis during excavation, subsequent analysis and documentation at various sites, the more temporally and laterally robust the regional biochronological framework becomes. Due to the abundance of faunal remains at DMK, we emphasise the role that faunal analysis has played in approximating early depositional ages for the site.

The DMK faunal sample published by Rovinsky et al. (2015) consists of faunal material recovered from the DMK-MM in 2013 and DMK-EM in 2014; although few remains were also recovered from the Southern Makondo (DMK-SM) (Fig. 2). Due to the density of fossils in DMK-EM excavations had only progressed some 20 cm in depth over an area with a diameter of ~1 m by the end of 2014. The heavy accumulation of fossils within the DMK-EM is related to its position against the eastern dolomite wall of the cave, into which more buoyant bones and fine sediments would have been winnowed (Pickering et al., 2007). This is also likely a product of the fact that it is a hollow within the breccia itself, therefore is in the early phases of decalcification. Other decalcified pockets at the site have also been correlated with a high density of fossils. We emphasise here that it is important to identify such effects during

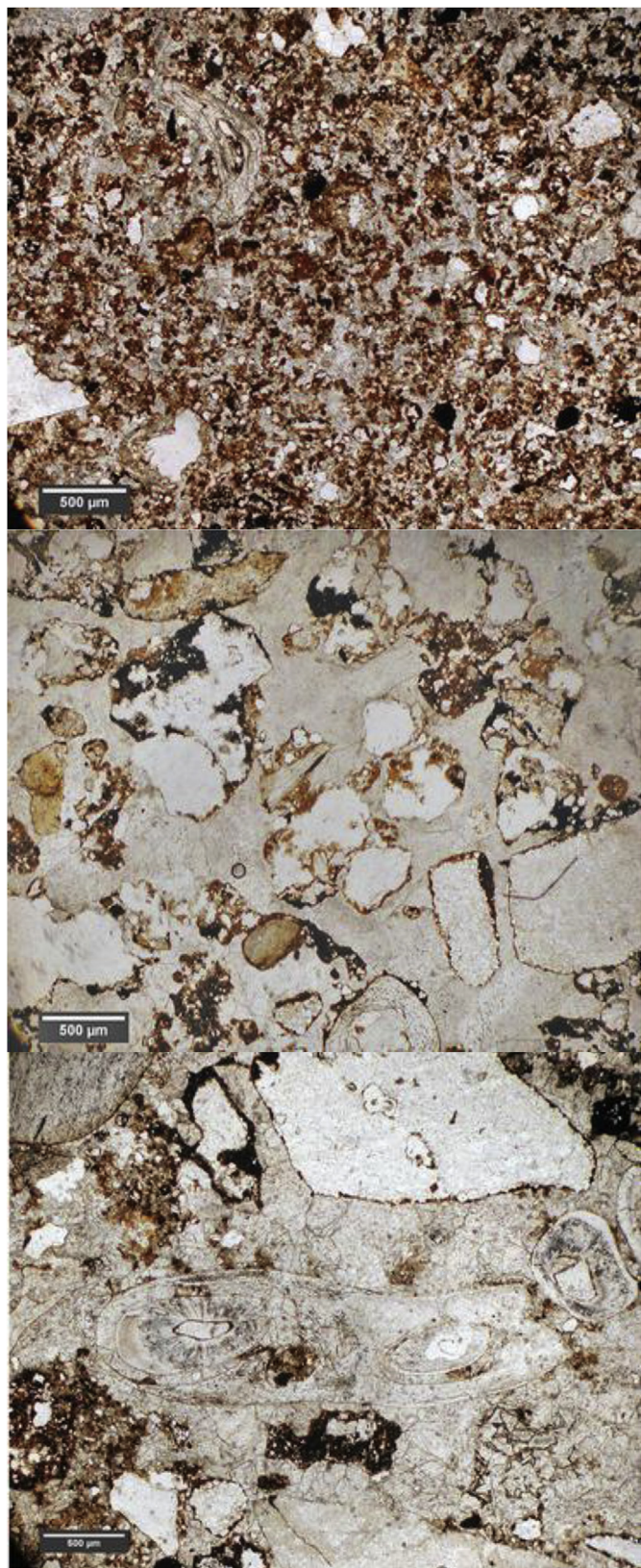


**Fig. 7.** A) top: Fine granular microstructure with enaulic coarse/fine related distribution pattern, strongly cemented by medium-size dirty sparite crystals. Few fine-to medium sand-size monocrystalline and very few polycrystalline quartz. Fe-oxide coatings cover some coarse grains (upper centre and upper right). Frequent rounded aggregates of fine material, stained by Fe-oxides. One altered bone fragment (upper left). PPL, 2.5 $\times$  objective. B) middle: Single-grain microstructure, with very fine

excavation and 3D plotting with a total station so that they can be considered during subsequent taphonomic analyses. Remains include a primate lower limb (base of DMK-WM), as well as other articulated carnivore and primate fossils found in direct association with fine grained sediments, indicating that animals had primary access to the cave. This is further emphasised by the lateral deposition of deposits (see 4.2.), which indicates no 'death trap' formed through a high vertical cave entrance as so often suggested for deposits with abundant articulated remains (e.g. Dirks et al., 2010).

The faunal analysis methods and detailed discussion is provided in Rovinsky et al. (2015) and only briefly summarized here with an emphasis on our biochronological interpretation. The DMK *Dinofelis* specimens are metrically and morphologically dissimilar to specimens from the younger Drimolen Main Quarry (DMQ) deposits (Rovinsky et al., 2015), which had been previously assigned to *Dinofelis* aff. *piveteaui* (O'Regan and Menter, 2009). However, Adams et al. (2016) have recently identified two different species from the DMQ, *Dinofelis* cf. *barlowi* and *Dinofelis* aff. *piveteaui*, the latter being similar to those from Cooper's D sometime between ~1.6 and <1.4 Ma. The genus *Dinofelis* is known from South African deposits ranging in age from the Langebaanweg Quartzose Sand Member at ~5.25–5.05 Ma (Roberts et al., 2011) to Cooper's D at 1.6–<1.4 Ma (de Ruiter et al., 2009). Other than perhaps the DMK, all specifically-attributable *Dinofelis* *barlowi* specimens are known from sites in the region that are older than ~2.0 Ma (e.g., Bolt's Farm Pit 23, Sterkfontein Members 2 and 4, and Malapa; Herries et al., 2009; Dirks et al., 2010; Werdelin and Peigné, 2010; Pickering et al., 2011a/b; Herries and Adams, 2013). The age of the sites (Motsetse, Kromdraai A, Coopers D) with specimens assigned to or with similarities to *Dinofelis* *piveteaui* (Lacruz et al., 2006) are all undated beyond biochronology (which is biased by the use of this species to suggest a younger age) other than Cooper's D at 1.6–<1.4 Ma (de Ruiter et al., 2009). Thus, these sites have generally been suggested to be younger due to *D. piveteaui*'s younger age in East Africa (Werdelin and Ewer, 2001) and the age of the Cooper's D material. While the range of ages contained in the DMQ is not currently known and thus the two did not necessarily overlap, the discovery of both these species in the DMQ deposit may not mean it is as good a chronological indicator of pre and post ~2 Ma deposits, as has been traditionally inferred; especially given the few specimens of the genus known from the region.

A *Metridiochoerus* specimen (DNM 57) is a maxillary third premolar that is a somewhat useful preliminary biochronological indicator for the DMK palaeocave deposit. It is morphologically and metrically aligned with early *Metridiochoerus andrewsi* specimens from the Makapansgat Member 3 deposits (3.03–2.58 Ma; Cooke, 2005; Rovinsky et al., 2015; Herries et al., 2013), as opposed to specimens from post ~2 Ma to ~1.8 Ma sites like Gondolin and Swartkrans (Herries et al., 2006a; b; Adams et al., 2007; Adams, 2010; Herries and Adams, 2013). While Makapansgat Member 3 represents the first definitive FAD (first appearance date) for *M. andrewsi* in South Africa, it also represents the most definitive LAD (last appearance date) of the more primitive Stage I (sensu Harris and White, 1979) *M. andrewsi* population. The actual LAD of this more brachydont *M. andrewsi* group can only currently be inferred by the occurrence of the more derived (Stage III)

fraction organised in enaulic related distribution pattern. Coarse-to very coarse sand-size chert grains, moderately altered. Discontinuous Fe/Mn-oxide coatings over almost all grains. Few Fe/Mn-oxide infillings in cracks within mineral grains. One slightly altered bone fragment (bottom, centre). PPL, 2.5 $\times$  objective. C) bottom: Moderately altered bone fragment; micromammal mandible, with in situ upper part of tooth roots. Coarse sediment, including very coarse sand-size chert grains and few aggregates of fine material. Thin Fe-oxide coatings on mineral grains. Anhedral to subhedral sparite cement, locally forming a pavimentous pattern with triple joints PPL, 2.5 $\times$  objective.

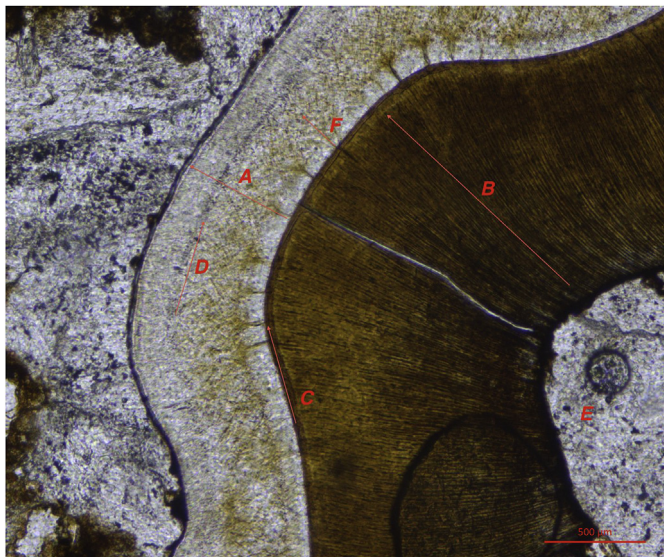


**Fig. 8.** Micromorphological thin section showing the structure of a micromammal tooth embedded within the Makondo siltstones. The tooth has been cemented within the breccia by sparitic calcite, with zones stained extensively by iron oxides (refer: far bottom left). Micromammalian tooth structures are outlined on the image and are described as follows; A) Enamel; B) Dentine (note: also showing Dentine Tubules along similar orientation to the arrow); C) Enamel Dentine Junction (EDJ); D) Potential Neonate Line; E) Pulp Cavity and F) Striae of Retzius.

*M. andrewsi* within deposits prior to Swartkrans Member 1 and Gondolin GD 2 (Herries et al., 2006b; Adams, 2010). Gondolin GD2 is dated between 1.95 and 1.78 Ma, although likely closer to 1.8 Ma (Herries et al., 2006b; Adams et al., 2007; Herries and Adams, 2013), where Swartkrans Member 1 has an expected age range between 2.0 and 1.8 Ma (Pickering et al., 2011; Herries and Adams, 2013). Unfortunately, this species lacks a robust data range from Sterkfontein and as aforementioned, few sites cover age ranges between terminal phases of deposition of the Makapansgat Lime-works Member 3 and Swartkrans Member 1 and Gondolin. This is with the exception of earlier internal parts of Gladysvale from ~2.4 Ma (Herries et al., 2013) and Haagst from ~2.33 to 1.95 Ma (Herries et al., 2014). In conclusion, while the DMK *Metridiochoerus* specimen is most comparable to specimens from Makapansgat prior to 2.6 Ma, an age as young as 2.2–2.0 Ma cannot be ruled out simply due to a lack of comparable fossils from this period. However, we acknowledge here that the period between 2.6 and 2.0 Ma is perhaps more expected to contain the intermediate Stage II *M. andrewsi* group, as seen in East African deposits (Cooke, 2007).

## 5. Geochronology

The last decade has seen the development of the uranium-lead (U-Pb) chronometer applied to speleothems and the ability to date material older than 500 ka (see Woodhead and Pickering, 2012 for a full recent review) which has had a profound impact on understanding the chronology of the South African palaeocave sites (Walker et al., 2006; de Ruiter et al., 2009; Pickering et al., 2010; Dirks et al., 2010; Pickering and Kramers, 2010; Pickering et al., 2011a; b). However, dating speleothems at a particular site often can only provide maximum or minimum ages for the fossil bearing deposits, depending on the spatial relationship between the speleothems and deposits of interest. Speleothems formed with a few hundred thousand years, or less, of each other may well have indistinguishable U–Pb ages given that the best errors achieved on such material is at best in the tens of thousands of years but more

typically in the 100ka range (Woodhead and Pickering, 2012). These limitations can be overcome by combining the U-Pb dating of speleothem with a detailed palaeomagnetic analysis of the full stratigraphy of the site and comparing the resulting magnetostratigraphic profile to the known Geomagnetic Polarity and Instability Time Scales (GPTS and GITS; Pickering et al., 2011b; Gradstein et al., 2012; Singer, 2014) using the U-Pb ages as tie points. The one disadvantage of this is that macromammalian remains occur at some sites exclusively in clast supported breccia deposits, to which palaeomagnetism cannot be reliably applied. Therefore, this method is not suitable to date sites unless fine-grained siltstone and sandstone deposits can be stratigraphically correlated or speleothem measured instead (Herries and Shaw, 2011).

Early Electron Spin Resonance (ESR) dating of fossils from the South African palaeocaves (Blackwell, 1994; Curnoe et al., 2001) have also recently been found to be reliable when compared with combined U-Pb/magnetostratigraphic ages (Herries and Shaw, 2011; Herries and Adams, 2013). However, it is acknowledged, that some results have had large errors when applied to earlier time periods with similar antiquity to sites within the CoH. Using modern methods and mapping of uranium in the teeth to be dated with direct coupled uranium-series electron spin resonance (US-ESR) dating of fossil teeth, various methods can be interpreted alongside sedimentological and micromorphological work to provide a robust chronology for palaeocaves. The three methods are applied at DMK as part of this combined study.

### 5.1. Uranium- lead (U-Pb) dating

U-Pb dating was applied to the basal flowstone speleothem taken from the western wall of DMK-NWR (Figs. 2–3). Thin section and palaeomagnetic analysis of the basal speleothem indicates that it contains little to no detrital iron from sedimentary influx and has a sharp contact with the overlying fossil bearing deposits wherever it is exposed in section. It underlies the basal clast supported breccia in DMK-MM and DMK-EM and also overlies the earlier phase of wad formation documented in DMK-NWR (Figs. 3 and 5). It is thus a good candidate to provide a maximum age for the DMK deposits because it would likely have formed in a sealed cave environment before there was an entrance and the sediments infilled the cave. Thin sections of the speleothem demonstrate that it consists of two main phases of growth. The bottom half is composed of acicular aragonite needles that have undergone partial replacement by a fine-grained equant calcite mosaic (approximately 80% aragonite; 20% secondary calcite). The top half is composed of a mosaic of equant calcite crystals with abundant aragonite needle relics, indicative of the diagenetic alteration of aragonite to calcite. As outlined in detail by Pickering et al. (2010) there is a small degree of recrystallisation in all CoH flowstones. This however is early (during growth of the speleothem in many cases), is conservative (no loss or gain of isotopes) and partial (much of the aragonite remains), so does not have an adverse affect on the U-Pb dating. The layer that was chosen for dating has elevated U concentrations, clearly visible on a cm scale and was therefore chosen as the target for U-Pb dating. Had this sample undergone massive recrystallisation, this U would have moved (U is highly soluble in water) and be spread across the sample, and not be concentrated in a thin layer.

Previous work on dating South African early Pleistocene speleothems has highlighted the necessity for some kind of pre-screening of samples, prior to dissolution and chemical analysis, in order to identify and target layers with uranium concentrations of  $\geq 1$  ppm ( $\mu\text{g/g}$ ) U (Pickering et al., 2010; Woodhead and Pickering, 2012). Phosphor-imaging, using a FUJIfilm BAS-1800

betascanner device, was used to map zones of higher radiation (attributed to higher U concentrations) within DMKPM05 (see Pickering et al., 2010 for more details; Fig. 4). Using this image as a guide, the layer richest in U was selected and a hand held dentist drill used to cut out small, ~3 mm<sup>3</sup> sub-sample blocks. These were then lightly etched using dilute HCl to remove any surface contamination from drilling and subsequent handling. From here onwards all laboratory work was conducted in a class 350 clean room, details of which are given in Woodhead et al. (2006, 2012). A mixed <sup>235</sup>U-<sup>205</sup>Pb spike was used and samples were measured on a Nu-Instruments MC-ICP-MS, again following Woodhead et al. (2006).

Element concentrations and isotope ratios obtained are summarized in Table 1. The average U concentration of DMKPM05 is 1.56 ppm (μg/g), with much lower Pb concentrations averaging at only 0.006 ppm. <sup>238</sup>U/<sup>206</sup>Pb ratios are relatively low, but there is enough spread to produce a range of <sup>207</sup>Pb/<sup>206</sup>Pb ratios and form robust Tera-Wasserberg isochron constructs (Fig. 12). The high MSWD of 37 reflects the scatter of these points around the slope. In samples such as DMKPM05, and indeed all of the other U-Pb dated flowstones from the GMD (Pickering et al., 2010; Pickering et al., 2011a; b), the initial <sup>234</sup>U/<sup>238</sup>U must have been >1 and must therefore be taken into account when calculating the age. If not ages tend to be over-estimated. The residual <sup>234</sup>U/<sup>238</sup>U excess in DMKPM05 was still measurable, <sup>234</sup>U/<sup>238</sup>U ratios were obtained following the protocol outlined in Pickering et al. (2011a) (Table 1). The slope from the Tera-Wasserberg isochron constructs (Fig. 12) and the residual <sup>234</sup>U/<sup>238</sup>U ratios (Table 2) are used to calculate a final U-Pb ages of 2.664 ± 0.392 Ma.

## 5.2. Coupled uranium-series electron spin resonance (US-ESR)

### 5.2.1. Sample preparation

A fragment of undiagnostic fossil bovid molar tooth (DMKESR04) was recovered from palaeomagnetic block sample DMK-PM02 during sampling. This sample comes from the very top of the DMK exposures (Figs. 3 and 6). The recovery of such fragments from breccia is ideal in these palaeocave deposits because the teeth have not undergone complex decalcification and thus have more homogenous dosimetry (Herries and Shaw, 2011). DMKESR04 consisted of a quarter of the molar with large piece of enamel (1.5 cm large and 3 cm long) and dentine attached (about 0.5 cm thick). The enamel was slightly discoloured at the surface, but with very few cracks and no infiltration of dirt despite being in direct contact with the surrounding sediments. The tooth fragment was removed from the block sample with a diamond wheel saw and the enamel was cleaned and stripped of the first 100 μm on both sides (the Enamel-Dentine Junction (EDJ) and the occlusal surface), while the dentine directly in contact was used for U and Th content.

**Table 1**

All U-Pb concentration and isotope ratio data used to calculate U-Pb ages for Drimolen Makondo flowstones sample DMKPM05. Errors are presented at 2 Sigma.

Sample	U ppm	Pb ppm	<sup>238</sup> U/ <sup>206</sup> Pb	% err	<sup>207</sup> Pb/ <sup>206</sup> Pb	corr. coef. 8/6–7/6	<sup>238</sup> U/ <sup>204</sup> Pb	% err	<sup>206</sup> Pb/ <sup>204</sup> Pb	% err	corr. coef. 8/4–6/4	
DMK5-1	1.387	0.015	277.7	1.0	0.678	0.1	-0.9999	7487.9	5.9	26.96	5.8	0.9864
DMK5-2	1.007	0.004	623.1	2.7	0.516	2.1	-0.9871	20951.9	7.7	33.63	6.2	0.9490
DMK5-3	1.571	0.005	763.9	3.9	0.453	3.9	-0.9994	26677.2	8.7	34.92	5.5	0.9549
DMK5-4	1.917	0.009	560.3	1.5	0.532	1.0	-0.9366	16648.6	2.8	29.71	1.5	0.9100
DMK5-5	2.265	0.007	710.4	3.0	0.460	2.9	-0.9995	24667.4	6.3	34.72	3.6	0.9718
DMK5-6	1.454	0.003	955.4	8.5	0.328	15.1	-0.9998	55287.0	29.7	57.87	21.5	0.9958
DMK5-7	1.318	0.002	1019.3	2.2	0.310	4.3	-0.9996	56197.8	7.3	55.13	5.1	0.9967
Ave.	1.560	0.006										

**Table 2**

Residual <sup>234</sup>U/<sup>238</sup>U ratios and final U-Pb ages of 2.664 ± 0.392 Ma for Drimolen Makondo basal flowstone sample DMKPM05.

Present <sup>234</sup> U/ <sup>238</sup> U	U-Pb (T-W)			% Error	Initial	
	±	% err	age (Ma)		±	<sup>234</sup> U/ <sup>238</sup> U
1.0023	0.0024	0.2	<b>2.664</b>	<b>0.392</b>	<b>14.715</b>	5.336
						2.487

### 5.2.2. Methods

US-ESR dating was performed on a Freiberg MS5000 X-band at 1G modulation amplitude, 2 mW power, 100G sweep, 100 kHz modulation frequency, coupled to a Varian VF50 X-ray irradiation chamber at 40 KV voltage and 0.5 mA current with dose rate averaging 0.24 Gy/s. The sample was mounted onto a Teflon sample holder, which expose directly the fragment to the x-ray source with no shielding (other than a 200 μm aluminium plate). Dose response curve (DRC) and equivalent dose (De) were calculated using the McDose 2.0 program from Joannes-Boyau et al. (2018). The DRC was calculated on the entire US-ESR dataset using a DSE. Associated errors were checked for strong aberration from 2-sigma of the average associated error. A 6% uncertainty was added to the De error obtained from the DRC to account for systematic error observed with x-ray. The amount of unstable radical (NOCORs) present in the sample was estimated based on the work by Joannes-Boyau and Grün (2011).

### 5.2.3. Dose rate

The external dose corresponds to the environmental (U, Th and K concentration in the sediment surrounding the tooth) dose rate (DSed) and the cosmic dose rate (Dcos). The DSed was measured for an average of 1h30min using a portable gamma spectrometer Inspector 1000, at three different locations at DMK in 2014 and 2015. The dose rate used was the one closer to the sample collected, while other values were used to estimate the intra-variability of the site as well as annual variability. The error associated took into account both variability, inducing a large error on the DSed. Because the breccia was so hard it was impossible to drill a hole sufficiently large for the probe to enter and because of the density of bone at DMK we did not want to do this for fear of damaging insitu fossils. All measurements were made in places where natural solution pockets occurred in the breccia. Since the probe was not surrounded by 30 cm of sediment (\* in Table 3), the peaks were integrated and modelled using the sedimentary configuration around the probe, inducing a large error on the measurements. Additionally, the sediment surrounding the sample was measured by ICPMS solution. The values obtained on the other location were used with the sediment values to have a general idea of the site dosimetry.

The DMK cosmic dose rate was rather complex to estimate because so much of DMK has been eroded away, making it difficult

to model properly. Using cosmogenic nuclide exposure dating the denudation rate was estimated to be in the order of 10 m per million years based on measurement of a quartz layer above the site (David Fink pers. com. 2018). It is obvious that this represent an estimation of the process, as the tooth could have been exposed gradually. However, the nature of the cave suggests the tooth was likely shielded by a chert cap cave rooftop for much of the time since its deposition, although this has now been eroded away. To be conservative we modelled the Dcos ( $t$ ) from two models (i) one the tooth was largely exposed to cosmic rays or (ii) the tooth was mostly shielded until recent time. This gave an average Dcos of  $220 \pm 65 \mu\text{Gy/a}$  and an average density of  $2.69 \pm 0.5 \text{ g cm}^{-3}$  for the breccia that was collected from the site. It includes a large error to account for large variability of the sediment. The density of the dolomite was calculated at  $2.85 \pm 0.03 \text{ g cm}^{-3}$ .

Internal dose was modelled using a LA-MC-ICPMS Neptune Plus by measuring uranium and thorium concentration directly in the enamel fragment used for US-ESR dating, as well as in the dentine directly attached. Furthermore, both enamel and dentine sections of the tooth were mapped to account for intra-variability, and a better understanding of diffusion processes overtime. Baseline and drift were corrected using a NIST 612, while ratios and concentrations corrected using two coral standard of known concentration. To account for potential matrix effect, a small fragment of dentine was also measured by ICPMS solution. Each measurement correspond of twelve separated rasters of  $700 \mu\text{m}$  long and  $200 \mu\text{m}$  wide laser spot following the growth of the dental tissues. Values measured show consistent results across the dentine and enamel sections.

To estimate the dose equivalent ( $De$ ), the sample was irradiated

nine times, following an exponential irradiation time (90s, 380s, 1080s, 1800s, 3600s, 7200s, 14700s, 28800s and 63300s). The dose response curve was calculated using the MCDose 2.0 with a Double Saturated Exponential DSE. For every irradiation steps the fragment was measured over  $180^\circ$  on the z-configuration (Joannes-Boyau and Grün, 2011). Isotropic and baseline correction was applied uniformly across the spectra. The amount of NOCORs in the natural signal of the DMK sample was estimated to be around  $13\% \pm 2$  using the angular measurements (Joannes-Boyau, 2013). As described by Grün et al. (2012), the amount of NOCORs did not fluctuate beyond the estimation uncertainty, after x-ray irradiation steps. The powder simulated values are calculated by averaging the values over the angular measurements of the z-configuration (Table 3).

#### 5.2.4. US-ESR results

The age of the DMK tooth was calculated to be  $2.706 \pm 0.428 \text{ Ma}$  (between 3.13 and 2.28 Ma; Table 3). Dating  $>\sim 1 \text{ Ma}$  fossils is challenging and several assumptions limit the precision and ultimately the accuracy of the US-ESR ages (Duval et al., 2011; Duval and Grün, 2016). The large error (Table 3) comes from the external dose calculation and the uranium uptake model. While, the U-series sample appears to be at equilibrium in the dental tissue, the uptake history prior to becoming a 'close system' is unknown leading to massive uncertainty in regards to age calculation. To reduce the error of the external dose in future dating of such deposits, and long term in-situ dosimeter should be used, as well as conducting a detailed geochemical characterisation of the breccia along the stratigraphic layers surround the tooth.

#### 5.3. Palaeomagnetic analysis

Palaeomagnetic analysis follows procedures outlined in Herries and Shaw (2011) and Herries et al. (2014). Samples were taken from fine-grained, horizontally stratified sediments on the walls of the Main Makondo deposit (DMK-PM01, 02, 04), as well as directly overlying the basal flowstone (DMK-PM03) and the results are presented in Table 4. The flowstone itself records a weak normal polarity, although it is so weak it is not considered reliable data. The siltstone samples from DMK are highly unusual for samples from South African palaeocave deposits in that they contain a number of components of magnetisation and thus it is assumed the different components are held by a variety of minerals and grain sizes (Fig. 9). The remanence is removed in the samples across a range of unblocking temperatures with Curie points around  $580^\circ\text{C}$  (Fig. 9E–F), suggestive of purer magnetite, as well as temperatures as low as  $470^\circ\text{C}$  (Fig. 9A, C), suggestive of titanomagnetite and/or maghaemite (Dunlop and Özdemir, 1997). Such low Curie points are not a common feature of South African palaeocave deposits, which are normally held exclusively by purer single domain to pseudo-single domain magnetite (Herries et al., 2006a; b; Adams et al., 2007; Herries and Shaw, 2011). Frequency dependence of magnetic susceptibility was undertaken using a Bartington MS2 Magnetic Susceptibility meter. Like other cave sites the DMK samples contain a high percentage of viscous grains across the single domain to superparamagnetic grain sized boundary (Herries et al., 2006a; b; Adams et al., 2007; Herries and Shaw, 2011) with  $\chi_{FD}\%$  values of 8.95–10.82%.

To further characterise this unusual behaviour and to confirm the measured remanence as related to primary formation a range of additional mineral magnetic experiments were undertaken (Fig. 10). Rock magnetic measurements were conducted on DMK samples to characterise the Fe mineral phase, domain state, and grain size of remanence carrying minerals. High temperature mass-specific magnetic susceptibility ( $\chi_T$ ) measurements were undertaken in air from room temperature to  $700^\circ\text{C}$  using a Geofyzika

**Table 3**

Combined US-ESR ages and associated data. The age was calculated using the  $^{234}\text{U}$  and  $\text{ThO}$  decay from Cheng et al. (1998), the enamel and dentine density of 2.95 from Grün (1986), alpha efficiency factor of  $0.15 \pm 0.02$ ,  $^{238}\text{U}$ - $^{234}\text{U}$  alpha dose ( $260 \text{ mGy/ka}$ ) from Grün (1987),  $^{230}\text{Th}$ - $^{234}\text{U}$  alpha dose ( $295 \text{ mGy/ka}$ ) from Grün and Invernati (1986), and an average sediment density of  $2.69 \pm 0.04 \text{ g.cm}^{-3}$ . Data and Ages are expressed with a 2-sigma error.

SAMPLE	DMK
<b>ENAMEL</b>	
Dose (Gy)	$2107 \pm 143$
U (ppm)	$1.46 \pm 0.24$
$^{234}\text{U}/^{238}\text{U}$	$1.4134 \pm 0.0649$
$^{230}\text{Th}/^{234}\text{U}$	$0.8076 \pm 0.0093$
Thickness (m)	$950 \pm 147$
Water (%)	$3 \pm 1$
<b>DENTINE</b>	
U (ppm)	$19.19 \pm 1$
$^{234}\text{U}/^{238}\text{U}$	$1.2018 \pm 0.0094$
$^{230}\text{Th}/^{234}\text{U}$	$0.8882 \pm 0.0165$
Water (%)	$5 \pm 3$
<b>SEDIMENT</b>	
U (ppm)	$0.65 \pm 0.22$
Th (ppm)	$1.35 \pm 0.45$
K (%)	$0.21 \pm 0.19$
Water (%)	$15 \pm 10$
<b>EXTERNAL DOSE</b>	
Beta Dose ( $\mu\text{Gy a}^{-1}$ )	$31 \pm 17$
Gamma Dose ( $\mu\text{Gy a}^{-1}$ )	$335 \pm 68$
Cosmic ( $\mu\text{Gy a}^{-1}$ )	$220 \pm 65$
<b>INTERNAL DOSE</b>	
Internal dose rate ( $\mu\text{Gy a}^{-1}$ )	$116 \pm 78$
Beta Dose rate dentine ( $\mu\text{Gy a}^{-1}$ )	$77 \pm 52$
P enamel	$4.6359 \pm 0.7708$
P dentine	$1.8967 \pm 0.3315$
Total Dose rate ( $\mu\text{Gy a}^{-1}$ )	$779 \pm 134$
<b>COMBINE US-ESR AGE</b>	
AGE (ka)	$2706 \pm 428$

**Table 4**

Palaeomagnetic Data for the Drimolen Makondo Palaeocave deposits.

Sample	Declination (°)	Inclination (°)	Mean MAD	K	Sample Number	VGPLat.	Polarity
DMK02	160.9	9.6	8.05	77.3	3	-62.0	R
DMK04	190.2	39.2	6.20	163.6	3	-79.9	R
DMK01	276.4	25.2	4.48	26.2	6	-2.8	I
DMK03U	142.1	-66.9	4.23	59.4	3	-7.3	I
DMK03L	47.9	-66.5	8.00	17.9	3	46.5	N

KLY-2 KappaBridge AC Susceptibility Bridge. Curie temperatures ( $T_c$ ) were calculated from the minimum in the first derivative of the  $\chi_T$  heating curve. Low temperature remanence and magnetic susceptibility measurements were undertaken with a Quantum Designs Magnetic Properties Measurement System XL. Samples were subject to a Field Cooled-Zero Field Cooled (FC-ZFC) experiment, involving sample cooling from 300 K (room temperature) to 20 K in a 2.5 T field, with remanence measurements taken at 5 K intervals in zero field upon warming (FC). This sequence was then repeated with the cooling procedure taking place in zero field (ZFC). Subsequently, a room temperature saturation isothermal remanent magnetisation (RT SIRM) of 2.5 T was applied and remanence measurements were undertaken over 300–20–300 K temperature sweeps at 5 K intervals. Magnetic susceptibility measurements were then undertaken upon warming from 20 to 300 K at frequencies of 1.0 Hz, 10.0 Hz and 99.0 Hz in 20 K intervals. First-order reversal curves (FORCs), hysteresis loops and remanence backfields were measured on a Princeton Measurements MicroMag Vibrating Sample Magnetometer. FORCs were processed using the FORCinel 3.0 software package (Harrison and Feinberg, 2008) and the VARIFORC smoothing protocol (Egli, 2013). Statistical unmixing of coercivity contributions to remanence backfield curves was undertaken using the web application MAX UnMix (Maxbauer et al., 2016). All other rock magnetic analyses were preformed using IRMDB software produced in-house at the Institute for Rock Magnetism.

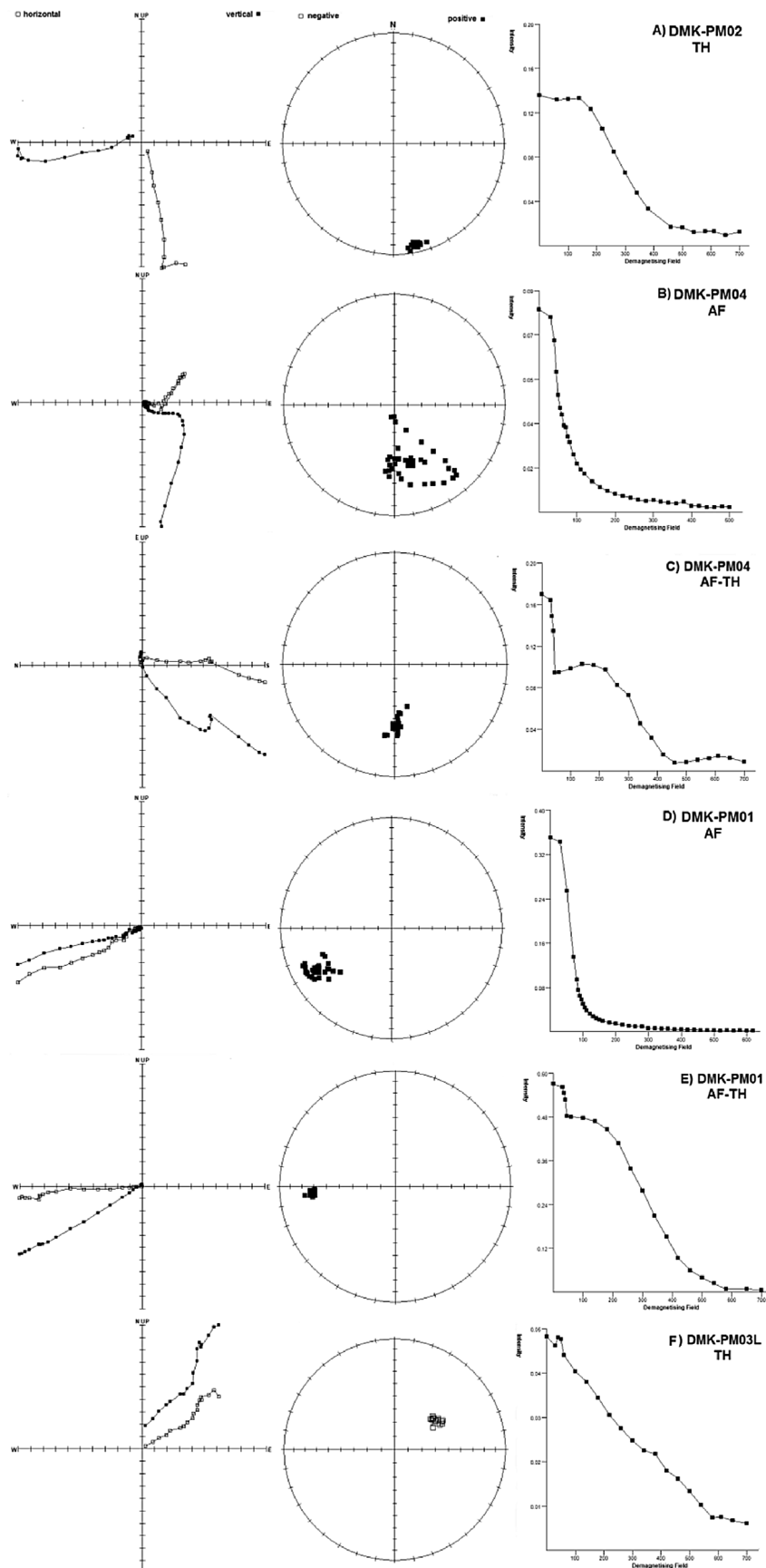
Results from the backfield unmixing (Fig. 10A) and FORC diagram (Fig. 10B) for DMK-02-A show that the bulk of the magnetisation is carried by low coercivity magnetic grains ranging from the ultrafine, to single domain (SD) and pseudo single domain (PSD) size ranges. There is no evidence for any multi-domain (MD) grain contributions as shown by minimal vertical spread along the  $B_u$  axis of the FORC (Roberts et al., 2000). This corroborates previous interpretations from South African palaeokarst (Herries et al., 2006a; b; Dirks et al., 2010; Herries and Shaw, 2011; Pickering et al., 2011a; b; Herries et al., 2014). Strong SD magnetisations are highlighted by closed concentric contours aligned along the FORC central ridge, while PSD contributors are shown by intensities with a broader spread away from the central ridge along the  $B_u$  axis and weak lobe-like features (Fig. 10B; Lascu et al., 2015; Roberts et al., 2000). SD and PSD grains likely correspond to the magnetisation imparted by Component 2 modelled within MAX UnMix, which largely fall within the coercivity ( $H_{cr}$ ) range of this dominant signal ( $H_{cr} = 19.81$  mT; Fig. 10A). Significant proportions of low coercivity ultrafine magnetic grains are not uncommon from these sites (e.g. Herries et al., 2006a; b; Herries and Shaw, 2011), and are illustrated via Component 1 of the coercivity distribution ( $H_{cr} = 1.74$  mT; Fig. 10A), along with a strong frequency dependence of magnetic susceptibility with temperature as highlighted in Fig. 10C. This component of the magnetisation is likely to be susceptible to secondary overprints, whereas SD, and to a lesser extent PSD particles, will be more likely to carry a stable remanent magnetisation.

Results from both  $\chi_T$  and low temperature remanence experiments indicate that the low coercivity magnetisations are carried by non-pure forms of magnetite. DMK-02-C records a  $T_c$  of

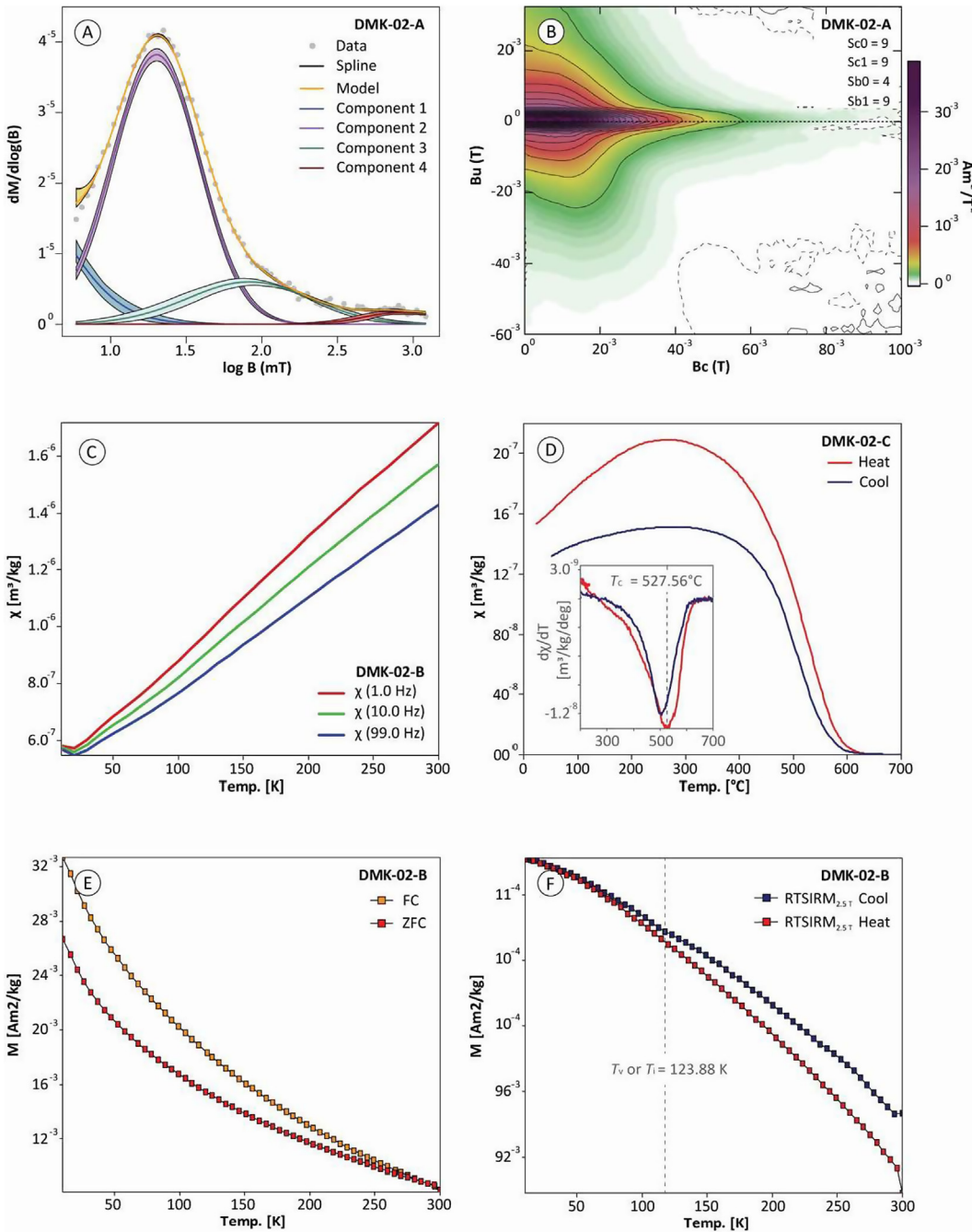
527.56 °C (Fig. 10D), significantly lower than the pure magnetite  $T_c$  of ~580 °C and lower than typical  $T_c$  estimates from these sites (which have been derived from thermomagnetic remanence cycles rather than  $\chi_T$  curves; e.g. Herries et al., 2006a, b and above). This may reflect titanium substitution (titanomagnetite) within the magnetite crystal lattice which causes a lowering of the  $T_c$  (Dunlop and Özdemir, 1997). A major difference at Drimolen is the occurrence of the large microgabbro deposit opposite the cave and this may explain the occurrence of titanomagnetite in the deposits. However, it could also potentially reflect the presence of maghemite, which can produce variable  $T_c$  values depending on the degree of oxidation effects (Dunlop and Özdemir, 1997). Low temperature data show a small inversion in the RT SIRM<sub>2.5 T</sub> cooling curve and loss in remanence close to the low temperature Verwey transition ( $T_v$ ; ~120 K) in magnetite (Fig. 10F). The  $T_v$  corresponds to a first-order phase transition in the crystal structure of magnetite from cubic to monoclinic which exhibits large diagnostic changes in the remanence observed during low temperature magnetometry (Dunlop and Özdemir, 1997). The  $T_v$  often occurs in a suppressed state, similar to the inversion noted in DMK-02-B, if partial oxidation or Ti-substitution has taken place (Moskowitz et al., 1998; Özdemir et al., 1993). In the case of the latter the  $T_v$  can be completely eliminated, although similar diagnostic features will remain at temperatures close to the  $T_v$  associated with magnetite's isotropic point ( $T_i$ ) (Moskowitz et al., 1998).

Fig. 10A also shows the presence of weak higher coercivity magnetisations, notably Component 4 which has a  $H_{cr}$  of 1367.4 mT indicating some antiferromagnetic mineral contribution. This is likely related to goethite, which has been identified via diagnostic low temperature properties in DMK-02-B. These include increases in magnetisation with lower temperatures (Fig. 10E and F), significant remanence differences between FC and ZFC curves (Fig. 10E) and largely reversible RT SIRM curves (Fig. 10F) (Lui et al., 2006). The remanence increases on cooling correspond to a decrease in magnetic susceptibility (Fig. 10C). Goethite has not previously been identified magnetically at these sites as this is the first application of low temperature remanence measurements. Antiferromagnetic components identified in SIRM experiments have typically been interpreted as haematite due to the red colouration of the sediments (e.g. Herries et al., 2006a; b). There does not appear to be any substantive evidence for a Morin transition in haematite (260–250 K) at low temperature within DMK-02-B (Fig. 10E and F), which similar to the  $T_v$  in magnetite, can be suppressed by increasing substitution as well when it occurs in ultrafine grain sizes (Dunlop and Özdemir, 1997). Evidence for a substantial amount of haematite is found in X-ray Absorption Spectroscopy analysis undertaken at the Australian Synchrotron (Fig. 11). This adds further support to the suggestion that haematite is a diagenetic product and is present largely in fine-grained pigmentary forms that is not remanence bearing, similar to its occurrence in burnt sediments (Herries et al., 2006a; b).

The large amount of ultra-fine grained ferrimagnetic grains identified in the samples has likely causes the strong, low coercivity overprints seen in the samples. Similar behaviours have been noted at other sites in the region that were easily removed using a hybrid



**Fig. 9.** Palaeomagnetic demagnetisation spectra (Zijderveld, Stereo, Intensity) for samples from Drimolen Makondo running from the base to the top of the stratigraphic sequence. A variety of sample behaviours and polarities are shown along with examples from the three different methods of demagnetisation (Alternating field; AF; Thermal; TH; and hybrid).



**Fig. 10.** Rock magnetic data for DMK-PM02 samples. A) MAX UnMix coercivity distribution of backfield measurements to  $-1.3 \text{ T}$ . B) FORC diagram composed of 132 individual FORCs with a smoothing factor of 4 for the central ridge (Sb0), and 9 for the remaining plot (Sc0, Sc1 and Sb1). Subtraction of the lower branch and removal of a first point artefact was undertaken during FORCinel processing. C) Low temperature magnetic susceptibility at three separate frequencies. D) High temperature magnetic susceptibility with a derivative plot insert. E) FC-ZFC low temperature data. F) RT SIRM low temperature data.

demagnetisation strategy with an initial 8–12 mT alternating field (AF) demagnetisation step before thermal demagnetisation (Dirks et al., 2010). Similar AF steps were used as part of a standard hybrid demagnetisation strategy for the Makondo samples. However, for the DMK samples this did not generally remove all the low field components in the samples (Fig. 9C). AF demagnetisation of DMK samples (Fig. 9B, D) indicate that potentially secondary overprints are not removed until a range of fields from 14 to 30 mT and that the samples have as many as 3 different components in some cases. This may relate to alteration noted by the

micromorphology, with secondary iron coatings to mineral grains. However, even where this is the case and the lower field components have been removed, a higher field stable remanence is recovered between 14/30–60 mT. Moreover, there is very little difference in the direction of the different components in most samples (Fig. 9D), suggesting they may have formed in different minerals at about the same time, rather than being more recent overprints. This is consistent with the occurrence of a range of unblocking temperatures identified during thermal demagnetisation. In a few samples (Fig. 9B) there is significant differences in

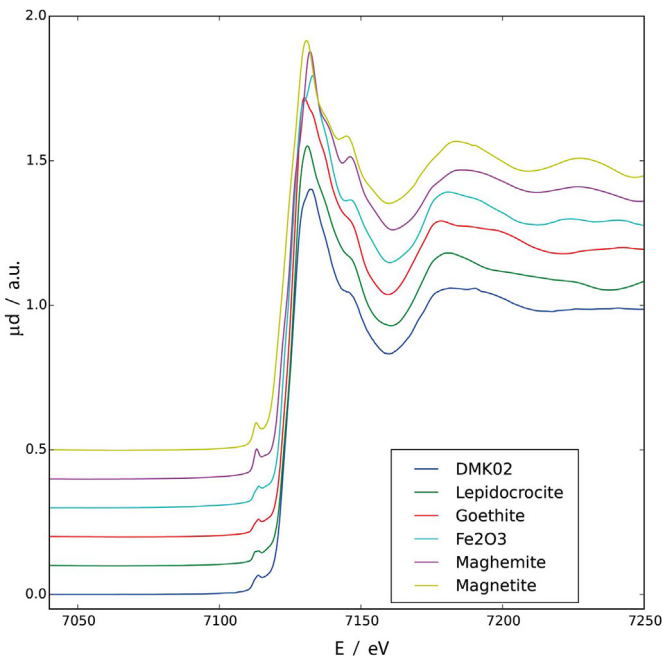


**Fig. 11.** X-ray absorption spectroscopy of DMK02 samples versus a range of magnetic standards. This indicates that the bulk iron mineral in the sample is haematite ( $\text{Fe}_2\text{O}_3$ ). This work was done at the Australian Synchrotron.

the direction of these lower field components that suggest they are more recently acquired overprints. In many samples a much higher temperature, very weak component also occurs, suggesting that haematite is also unusually holding a remanence. However, the inclination of the haematite remanence is identical in every single sample, with a characteristic almost vertical ( $-80$  to  $-90^\circ$ ) inclination and as such it is thought to be secondary in nature, perhaps related to the conversion of maghaemite to haematite. The stability of the characteristic remanence to high fields of 60 mT points to the occurrence of greater concentrations of larger stable single domain particles than seen at other sites and this is reflected in the mineral magnetic measurements. This is in theory the ideal magnetic carrier for a primary remanence. However, the above mineralogy suggests a complex mixture of magnetic minerals occur whereby an overprint is produced because the sediments formed rapidly during a reversal and minerals that took longer to lock the remanence into the sediment have a different direction to the primary single domain magnetite remanence. Some secondary diagenetic overprinting may also be evident, but this is removed during magnetic cleaning.

Block sample DMK-PM03, which sits against the flowstone records normal (VGP  $46.5^\circ$ ; Table 4) and intermediate polarities (VGP  $-7.3^\circ$ ) with subsamples having steep negative inclinations of  $-60.6^\circ$  to  $-85.7^\circ$ . Sample DMK-PM01, which sits above this in the base of the siltstone and sandstone phase also records intermediate polarities (VGP;  $-2.8$ ), but trending towards reversed polarity with positive inclinations ( $273.4^\circ/25.2^\circ$ ). DMK-PM04, which is slightly higher records completely reversed directions (VGP:  $-79.9^\circ$ ;  $190.2^\circ/39.2^\circ$ ) as does the very top of the sequence (DMK-PM02:  $160.9^\circ/9.6^\circ$ ; VGP:  $-62.0^\circ$ ). The data is consistent with a change in polarity from normal to reversed polarity occurring during the deposition of the deposits (Fig. 12). Similar reversal events have been found in other caves within the region, although they have most often been found within speleothem deposition (Adams et al., 2007; Dirks et al., 2010, 2017; Herries et al., 2013, 2014).

## 6. Discussion and conclusions

The close interdisciplinary relationship between earth sciences and archaeology has long existed in other parts of the world (Davidson and Shackley, 1976; Rapp and Hill, 2006; Stein, 2001; Waters, 1996; Waters and Kuehn, 1996), although has yet to be fully established as an integral part of South African palaeoanthropological research. This is an alarming notion as the geomorphological complexity of fossil-bearing palaeokarst is rarely given enough focus during research. Until only recently South African palaeocave deposits have largely been founded through the exploitation of lime mining throughout the 20th Century, which removes the geology and fossil material from primary context. This has greatly influenced how researchers have gathered contextual and chronological data for palaeoanthropological and archaeological material at the site; where many relied solely on biochronological frameworks. Many that have attempted to understand the depositional phases at these sites have adopted the 'Member System' (e.g. Partridge, 1978, 1979, 2000; Bruxelles et al., 2016); a simplistic concept unique to ascertain infilling stages in South African palaeokarst. However, as numerous researchers have noted (Latham et al., 1999, 2003; Pickering and Kramers, 2010; Herries et al., 2013) how classifying these palaeocaves sites based on a Member system is flawed as assumed temporal sequencing (i.e Member 1 as the oldest and 5 as the youngest) has been shown to not be the case at many sites (Latham et al., 2003; Pickering and Kramers, 2010; Bruxelles et al., 2016). This is mainly because 'Members' are classified based on their sedimentological character. However, caves are systems where very different processes and thus sedimentological processes can occur in different parts of the cave at the same time. Consequently, contemporary deposits have often been separated into different, supposedly temporal, units based on their sedimentological character. For example, Member 2 (siltstone and sandstone) and 4 (breccia) at the Makapansgat Limeworks are contemporary as Member 2 derives from the winnowing of Member 4 (Herries et al., 2013). Separating these two deposits into different temporal units based on sedimentology is like separating the Central Breccia at DMK and the adjacent siltstone and sandstone deposits into separate temporal deposits. This is clearly not justifiable. Other examples of this include Bruxelles et al., 2016 confusing reordering of the Members at Kromdraai B and the arguments over the age and relationship of Member 2 and Member 4 at Sterkfontein (Partridge, 1978, 2000; Walker et al., 2006; Partridge et al., 2003; Pickering and Kramers, 2010; Herries and Shaw, 2011; Herries et al., 2013; Bruxelles et al., 2014; Granger et al., 2015; Kramers and Dirks, 2017a,b).

One way that other researchers have tackled this problem is in defining chronostratigraphic units rather than sedimentological ones, often separated by flowstone speleothem and thus defined as Flowstone Bound Units (e.g. Pickering et al., 2007; Adams et al., 2010; Herries et al., 2014). Even this approach can be quite general and only through 3D mapping and with detailed stratigraphic analysis, both laterally and vertically, and combined with micromorphological analysis can the complex stratigraphy of these types of sites be confidently assessed.

More recent discoveries of sites such as Drimolen, Haasgat, Rising Star and Malapa (Dirks et al., 2017; Herries et al., 2017; Leece et al., 2016) have started to adopt more relevant contextual studies that are directly aligned with concepts with the earth sciences. These have been discussed in detail throughout this paper and it should be emphasised that this is the first example of all these tools applied together at one site. As presented here, these techniques should be carried out in order from regional studies; geological exploration and GPR, to site-specific; excavation and data collection. Lastly, a focus on substantial laboratory work including thin

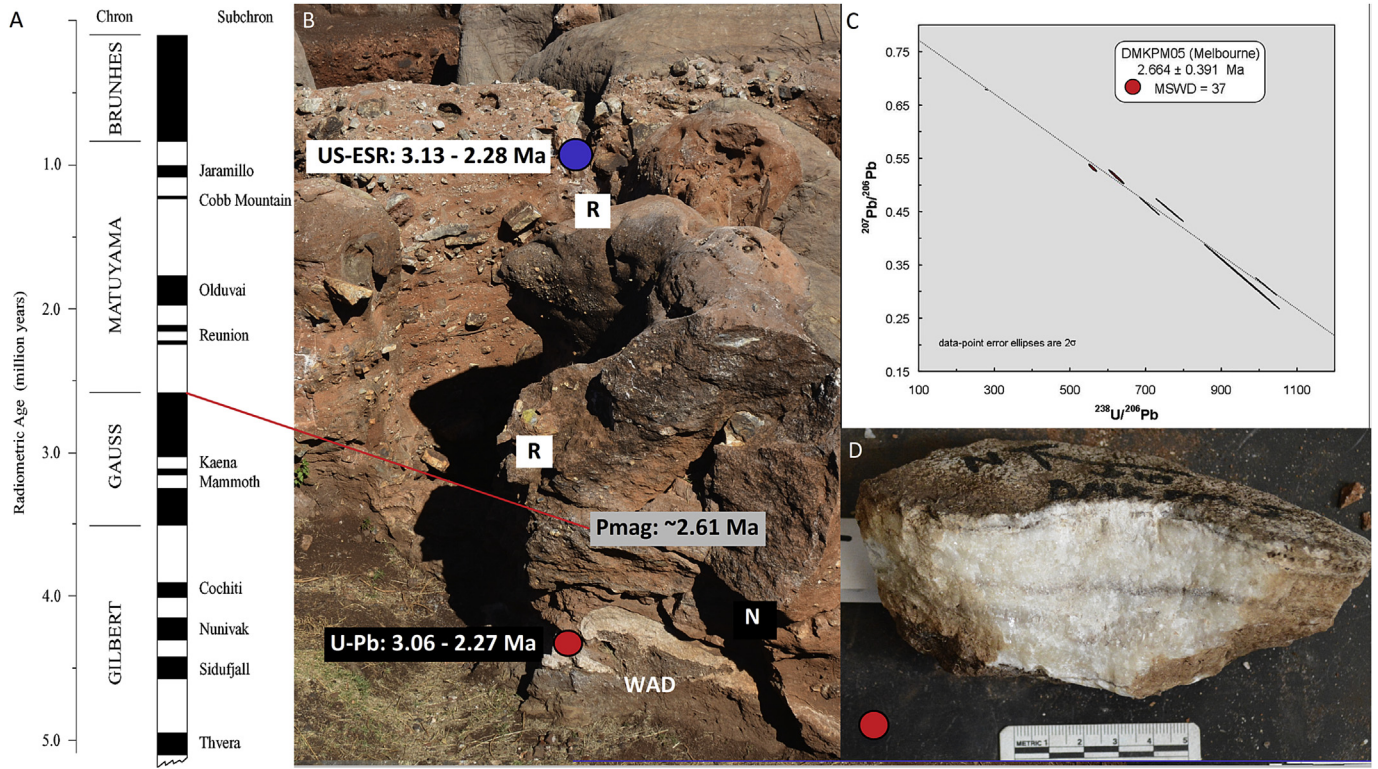


**Fig. 12.** A: Geomagnetic Polarity Timescale compared against B: the stratigraphic sequence of DMK showing the location and age estimate of U-Pb (red circle), US-ESR (blue circle) and Palaeomagnetic (N=Normal, R=Reversed) samples.; C: Tera-Wasserberg isochron age constructs for DMKPM05 from the Melbourne laboratory. The slope of this line and the measured  $^{234}\text{U}/^{238}\text{U}$  ratio are used to calculate ages; D: The DMKPM05 dated flowstone sample showing the dated basal aragonite rich part. (For interpretation of the references to colour in this figure legend, the reader is referred to the Web version of this article.)

section analysis, amalgamating excavation material for 3D modelling as well as a comprehensive utilisation of multiple dating techniques; palaeomagnetic analysis, US-ESR dating. By compiling data that is multi-sourced and analysed using an array of techniques, supporting information can be used to validate and corroborate conclusions drawn about the depositional history of the site. This is clearly important for providing context to fossils, ultimately placing them within our lineage.

At the DMK many of the articulated remains in the decalcified sediments from the edges of DMK-MM and DMK-EM continued into the still calcified sediments. This likely indicates that the fossil material present in the decalcified sediments is derived from the neighbouring calcified deposits and is not a mixture of older residual material with younger fossils. Although we argue that biochronological based contexts are insufficient to produce a confident chronological history of the site, it is still a powerful tool to be used in conjuncture with other dating methods. Particularly when specimens align with temporally defined populations. Although there were many different species identified in the DMK-EM, there were some species that could provide a time bracket for deposition; namely the *Metridiochoerus* specimen. This specimen (DNM 57) is likely derived from a Stage I *Metridiochoerus andrewsi* which has only been previously found in pre-2.6 Ma sites in South Africa (Rovinsky et al., 2015). However, we know very little about the period between 2.6 and 2.0 Ma because so few sites have been dated to this time period (Herries et al., 2009; Pickering et al., 2011a; b; Herries and Adams, 2013; Kuhn et al., 2016) other than Sterkfontein Member 4 (Pickering and Kramers, 2010; Herries et al., 2013). However, so little has been undertaken on the fauna from this site in recent years or from modern excavations.

The utilisation of various dating methods at DMK, combined

with a comprehensive understanding of depositional regimes, validated our conclusions that this site is of greater antiquity than the DMQ, which is dated to between 2.0 and 1.4 Ma (Herries et al., 2017). U-Pb dating on the basal flowstone unit exposed on the NWR (sample DMKPM05) indicate an age of  $2.644 \pm 0.391$  Ma (sometime between 3.035 and 2.253 Ma; Fig. 12). As magnetic and thin section analysis of this unit indicates minimal detrital material, it is surmised that this age is for the closed cave system, before roof collapse and infilling overlying fossil-rich units. The palaeomagnetic sequence suggests a change from normal to reversed polarity through intermediate polarity, with reversed polarity for the layer that contains the  $2.706 \pm 0.428$  Ma US-ESR age (sometime between 3.134 and 2.274 Ma; Fig. 12). The U-Pb and US-ESR age thus overlap within the period between 3.035 and 2.274 Ma. Only three magnetic reversals occur within this time range: 1) the end of the Kaena SubChron at ~3.03 Ma (Ogg, 2012, Fig. 12a), which is at the very upper limit of the age uncertainty and is reversing from reversed to normal polarity, rather than normal to reversed as in DMK; 2) the Halawa Excursion at ~2.445 Ma (Singer, 2014) that has also often been referred to as X-event. While this could represent the reversal in DMK, it is much more likely that it represents; 3) the Gauss-Matuyama Boundary reversal at ~2.61 Ma (Singer, 2014, Fig. 12). This reversal is from normal to reversed polarity and its age is close to the central age estimates from both the US-ESR and U-Pb dating. Moreover, it has been suggested by Pickering et al. (2011a, b) that synchronous flowstone formation occurs in several caves in the region and this is the same age as estimates for flowstone ages at the base of Sterkfontein Member 4, which subsequently also records reversed polarity (Herries and Shaw, 2011). Despite large age uncertainties for both the US-ESR and U-Pb methods, the combination of these two methods with palaeomagnetism has

allowed DMK to be dated to a period contemporary with the early phase of Sterkfontein Member 4 deposition, and provides further validation for using this combination of dating methods on these sites as they often correlate extremely well (Herries and Shaw, 2011; Herries and Adams, 2013; Dirks et al., 2017). By corroborating all these techniques, we are able to form a comprehensive, well-established chronostratigraphic profile at DMK.

As regional geological studies are beginning to identify new and untouched palaeoanthropological sites (Dirks et al., 2016; Herries et al., 2017), a more robust geoarchaeological framework for research on *in-situ* palaeokarst deposits is important. As aforementioned, many sites within the CoH have been actively mined for internal speleothem deposits, which causes partial or complete destruction of well-preserved stratigraphies. This can be worsened by extensive excavations that also removes sediment blocks from their original context, where incomplete or inconclusive field data can cause misleading interpretations when the site is revisited. Another concern, particularly when excavating makondo features, is the potentially high likelihood of mixing of fossils of different ages; as envisaged by Brink and Partridge (1980). This can occur due to direct decalcification of bone from the surrounding palaeocave deposits, as well as fossils being brought into drained makondo features due to later colluvial infilling. It is thus important to assess this when excavating a site, especially if no comparative *in-situ* palaeocave sediments are also being sampled for fossil extraction, as has been the case at several similar palaeokarst sites in the region. DMK presents a unique case study which assess chronology and formation history of a minimally impacted site which remains stratigraphically intact. Although *in-situ* deposits are typically simpler when interpreting contextual information, they present their own sets of issues. The first of these is uncovering them and removing colluvium safely and efficiently. GPR greatly enhanced our overall understanding of the DMK palaeocave system before excavations occurred; identifying the extents of the site as well as proving an important tool for ensuring safety precautions were in place getting closer to open cavities during excavations.

While research exists on the hominin-bearing palaeocaves, recent results from less intensively worked or new fossil localities in the northern sector of the CoH, highlight the importance of broader geological, technical and chronological studies. This case study at DMK not only presents a unique collaboration of techniques, it provides a unique example of a site that has not been heavily altered through modern anthropogenic activities. Approaches that have been outlined in this study are still relatively novel South Africa, particularly being used corroboratively at single site. Therefore, we argue this multi-stage, holistic geological approach will positively advocate for the utilisation of geoarchaeological methods, which is critical to aid in understand the formation of hominin-bearing palaeokarst and thus, the chronology and context of fossils identified within.

## Acknowledgments

The work at Drimolen has been funded by an Australian Research Council Future Fellowship FT120100399 to AIRH (2012–2016), an ARC Discovery Project DP170100056 to AIRH, JWA, and RJB and a La Trobe University Field School (2013–present). It has additionally been supported by La Trobe University Postgraduate Research Scholarships to BA, AB, TM, and AM and La Trobe University Internal Research Grants to BA, TM and AM. The Australian Archaeology Association has also supported this research by awarding a PhD Grant to AM. Rock magnetic experiments were undertaken during a Visiting Research Fellowship to TM at the Institute for Rock Magnetism (IRM), University of Minnesota, supported through the National Science Foundation, USA. We would

like to thank Dario Bilardello, Mike Jackson, and Joshua Feinberg for their assistance and advice while measuring at the IRM. Work at the Australian Synchrotron was funded by M12034, FI6084 and EU9516 beam time grants to AIRH, PK and TM. U–Pb speleothem dating was funded by an Australian Research Council DECRA fellowship (to RP; DE120102504), special thanks to Petra Bajo and John Hellstrom (University of Melbourne). The GIS, GPR and photogrammetry work was undertaken in VisLab2 at La Trobe University. Thanks to Stephany Potze, Lazarus Kgasi, Shaw Badenhorst (Ditsong National Museum of Natural History), Laura Abraczinskas (Michigan State University), and Bernhard Zipfel (University of the Witwatersrand) for facilitating access to the modern and fossil comparative faunal specimens housed at their institutions. Up until 2016 SAHRA permits for the work at Drimolen were held by Colin Menter and since 2017 by SB and AIRH. We would also like to thank the landowners (Mr Nathi Nkosi and Mr Khethi Nkosi) for allowing us to work at the site as well as the staff and students of the Drimolen Field Schools.

## References

- Adams, J.W., 2010. Taphonomy of the Gondolin GD 2 *in situ* deposits and its bearing on interpretations of South African Plio-Pleistocene karstic fossil assemblages. *J. Taph.* 8, 81–116.
- Adams, J.W., Herries, A.I.R., Hemingway, J., Kegly, A., Kgazi, L., Hopley, P., Reede, H., Potze, S., Thackeray, F., 2010. Initial fossil discoveries from Hoogland, a new Pliocene primate-bearing karstic system in Gauteng Province, South Africa. *South Afr. J. Hum. Evol.* 59, 685–691.
- Adams, J.W., Herries, A.I.R., Conroy, G.C., Kuykendall, K., 2007. Taphonomy of a South African cave: geological and hydrological influences on the GD 1 fossil assemblage at Gondolin, a Plio-Pleistocene paleocave system in the Northwest Province, South Africa. *Quat. Sci. Revs.* 26, 2526–2543.
- Adams, J.W., Rovinsky, D., Herries, A.I.R., Menter, C., 2016. Macromammalian faunas, biochronology and palaeoecology of the early Pleistocene main Quarry hominin-bearing deposits of the drimolen palaeocave system, South Africa. *PEERJ*. <https://doi.org/10.7717/peerj.1941>.
- Agisoft, 2013. Agisoft PhotoScan User Manual Professional Edition. Available at: Version 1.0.0. [http://downloads.agisoft.ru/pdf/photoscan-pro\\_1\\_0\\_0\\_en.pdf](http://downloads.agisoft.ru/pdf/photoscan-pro_1_0_0_en.pdf).
- Armstrong, B., Blackwood, A., Penzo-Kajewski, P., Menter, C.G., Herries, A.I.R., 2018. Terrestrial laser scanning and photogrammetry techniques for documenting fossil bearing palaeokarst with an example from the Drimolen Palaeocave System, South Africa. *Archaeol. Prospect.* 25, 45–58.
- Backwell, L., d'Errico, F., 2008. Early hominid bone tools from Drimolen, South Africa. *J. Arch. Sci.* 35, 2880–2894.
- Berger, L.R., et al., 2015. *Homo naledi*, a new species of the genus *Homo* from the Dinaledi Chamber, South Africa. *eLife* 4. <https://doi.org/10.7554/eLife.09560>.
- Benson, A.K., 1995. Applications of ground penetrating radar in assessing some geological hazards: examples of groundwater contamination, faults, cavities. *J. Appl. Geophys.* 33 (1–3), 177–193.
- Blackwell, B., 1994. Problems associated with reworked teeth in electron spin resonance (ESR) dating. *Quatern. Sci. Rev.* 13, 651–660.
- Brain, C.K., 1958. The Transvaal ape-man bearing cave deposits. *Transvaal Mus. Mem.* 11, 1–131.
- Brink, A.B.A., Partridge, T.C., 1980. The nature and genesis of solution cavities (Makondos) in Transvaal cave breccias. *Palaeontol. Afr.* 23, 47–49.
- Bruxelles, L., Marie, R., Couzens, R., Thackeray, J.F., Braga, J., 2016. A revised stratigraphy of Kromdraai. In: Braga, Thackeray (Eds.), *Kromdraai: a Birthplace of Paranthropus in the Cradle of Humankind*. Sun Press, pp. 31–48.
- Bruxelles, L., Clarke, R.J., Maire, R., Ortega, R.M., Stratford, D., 2014. Stratigraphic analysis of the Sterkfontein StW 573 *Australopithecus* skeleton and implications for its age. *J. Hum. Evol.* 70, 36–48.
- Chalikakis, K., Plagnes, V., Guerin, R., Valois, R., Bosch, F., 2011. Contribution of geophysical methods to karst-system exploration: an overview. *Hydrogeology J.* 19 (6), 1169–1180.
- Chamberlain, A.T., Sellers, W., Proctor, C., Coard, R., 2000. Cave detection in limestone using ground penetrating radar. *J. Archaeol. Sci.* 27 (10), 957–964.
- Cheng, H., Lawrence Edwards, R., Murrell, M.T., 1998. Uranium-Thorium-protactinium dating systematics. *Geochimica Cosmochimica Acta* 62, 3437–3452.
- Cooke, H.B.S., 2005. Makapansgat suids and *Metridiochoerus*. *Palaeontol. Afr.* 41, 131–140.
- Cooke, H.B.S., 2007. Stratigraphic variation in Suidae from the Shungura Formation and some coeval deposits. In: Bobe, R., Alemseged, Z., Behrensmeyer, A.K. (Eds.), *Hominin Environments in the East African Pliocene: an Assessment of the Faunal Evidence*, pp. 107–127. *Vertebrate Paleobiology and Paleoanthropology Series*.
- Curnoe, D., Grün, R., Taylor, L., Thackeray, F., 2001. Direct ESR dating of a Pliocene hominin from Swartkrans. *J. Hum. Evol.* 40, 379–391.
- Davidson, D.A., Carter, S.P., Quine, T.A., 1992. An evaluation of micromorphology as an aid to archaeological interpretation. *Geoarchaeology* 7 (1), 55–65.
- Davidson, D.A., Shackley, M.L., 1976. In: Davidson, D.A., Shackley, M.L. (Eds.),

- Geoarchaeology: Earth Science and the Past:(papers)]. Westview Press.
- de Ruiter, D.J., 2003. Revised faunal lists for Members 1e3 of Swartkrans, South Africa. *Annls. Transvaal Mus.* 40, 29–41.
- de Ruiter, D., Pickering, R., Steininger, C., Kramers, J., Hancox, P., Churchill, S., Berger, L., Backwell, L., 2009. New *Australopithecus robustus* fossils and associated U-Pb dates from Cooper's Cave (Gauteng, South Africa). *J. Hum. Evol.* 56, 497–513.
- de Ruiter, D.J., Brophy, J.K., Lewis, P.J., Churchill, S.E., Berger, L.R., 2008. Faunal assemblage composition and paleoenvironment of plovers lake, a middle stone age locality in Gauteng Province, South Africa. *J. Hum. Evol.* 55, 1102–1117.
- Dirks, P.H.D., Kibii, J.N., Kuhn, B.F., Steininger, C., Churchill, S.E., Kramers, J.D., Pickering, R., Farber, D.L., Mériaux, S.-A., Herries, A.I.R., King, G.C.P., Berger, L.R., 2010. Geological setting and age of *Australopithecus sediba* from southern Africa. *Science* 328, 205–208.
- Dirks, P.H.G.M., Placzek, C.J., Fink, D., Dosseto, A., Roberts, E., 2016. Using  $^{10}\text{Be}$  cosmogenic isotopes to estimate erosion rates and landscape changes during the Plio-Pleistocene in the Cradle of Humankind, South Africa. *J. Hum. Evol.* 96, 19–34.
- Dirks, P.H.G.M., Roberts, E.M., Hilbert-Wolf, H., Kramers, Hawks, J.D., Dosseto, A., Duval, M., Elliott, M., Evans, M., Grün, R., Hellstrom, J., Herries, A.I.R., Joannes-Boyau, R., Makhubela, T.V., Placzek, C.J., Robbins, J., Spandler, C., Wiersma, J., Woodhead, J., Berger, L.R., 2017. The age of *Homo naledi* and associated sediments in the Rising Star Cave, South Africa. *elife*. <https://doi.org/10.7554/elife.24231>.
- Dunlop, D.J., Özdemir, Ö., 1997. Rock Magnetism: Fundamentals and Frontiers, Cambridge Stud. Magn., vol. 3. Cambridge Univ. Press, New York.
- Duval, M., Grün, R., 2016. Are published ESR dose assessments on fossil tooth enamel reliable? *Quat. Geochronol.* 31, 19–27.
- Duval, M., Falguères, C., Bahain, J.-J., Grün, R., Shao, Q., Aubert, M., Hellstrom, J., Dolo, J.-M., Agusti, J., Martínez-Navarro, B., Palmqvist, P., Toro-Moyano, I., 2011. The challenge of dating Early Pleistocene fossil teeth by the combined uranium series–electron spin resonance method: the Venta Micena palaeontological site (Orca, Spain). *J. Quat. Sci.* 26, 603–615.
- Egli, R., 2013. VARIFORC: an optimized protocol for calculating non-regular first-order reversal curve (FORC) diagrams. *Glob. Planet. Change* 110, 302–320.
- FitzPatrick, E.A., 1984. The Micromorphology of Soils. Springer.
- Gosar, A., 2012. Analysis of the capabilities of low frequency round penetrating radar for cavities detection in rough terrain conditions: the case of Divača Cave, Slovenia. *Acta Carsologica* 1 (76), 41.
- Gommery, D., Badenhorst, S., Senegas, F., Potze, S., Kgasi, L., Thackeray, J.F., 2012. Preliminary results concerning the discovery of new fossiliferous sites at Bolt's Farm (Cradle of Humankind, South Africa). *Ann. Ditsong Natl. Mus. Nat. Hist.* 2, 33–45.
- Gradstein, F.M., Ogg, J.G., Schmitz, M., Ogg, G., 2012. The Geologic Time Scale. Elsevier, Boston.
- Granger, D.E., Gibbon, R.J., Kuman, K., Clarke, R.J., Bruxelles, L., Caffee, M.W., 2015. New cosmogenic burial ages for Sterkfontein member 2 *Australopithecus* and member 5 oldowan. *Nature* 522, 85–88.
- Grün, R., 1987. Alpha dose attenuation in thin layers. *Anc. TL* 5, 6–8.
- Grün, R., 1986. Beta dose attenuation in thin layers. *Anc. TL* 4, 1–8.
- Grün, R., Invernari, C., 1986. Uranium accumulation in teeth and its effect on ESR dating—a detailed study of a mammoth tooth. *Nucl. Tracks Radiat. Meas.* 10, 869–877.
- Grün, R., Mahat, R., Joannes-Boyau, R., 2012. Ionization efficiencies of alanine dosimeters and tooth enamel irradiated by gamma and X-ray sources. *Radiat. Meas.* 47, 665–668.
- Harris, J., White, T., 1979. Evolution of the plio-pleistocene african suidae. *Trans. Am. Phil. Soc.* 69, 5–128.
- Harrison, R.J., Feinberg, J.M., 2008. FORCinel: an improved algorithm for calculating first-order reversal curve distributions using locally weighted regression smoothing. *Geochem. Geophys. Geosystems* 9, Q05016. <https://doi.org/10.1029/2008GC001987>.
- Herries, A.I.R., Adams, J.W., 2013. Clarifying the context, dating and age range of the Gondolin hominins and *Paranthropus* in South Africa. *J. Hum. Evol.* 65, 676–681.
- Herries, A.I.R., Adams, J.W., Joannes-Boyau, R., Armstrong, B., Baker, S., Blackwood, A., Boshian, G., Caruana, M., Penzo-Kajewski, P., Murszewski, A., Rovinsky, D., 2017. Integrating palaeocaves into palaeolandscapes: an analysis of cave levels and karstification history across the Gauteng Malmani dolomite, South Africa. *Quat. Sci. Rev.* (in press).
- Herries, A.I.R., Adams, J.W., Kuykendall, K.L., Shaw, J., 2006a. Speleology and magnetobiostratigraphic chronology of the GD 2 locality of the Gondolin hominin-bearing paleocave deposits, North West Province, South Africa. *J. Hum. Evol.* 51, 617–631.
- Herries, A.I.R., Reed, K., Kuykendall, K.L., Latham, A.G., 2006b. Speleology and magnetobiostratigraphic chronology of the buffalo cave fossil bearing palaeodeposits, Makapansgat, South Africa. *Quat. Res.* 66, 233–245.
- Herries, A.I.R., Curnoe, D., Adams, J.W., 2009. A multi-disciplinary seriation of early *Homo* and *Paranthropus* bearing palaeocaves in southern Africa. *Quat. Int.* 202, 14–28.
- Herries, A.I.R., Hopley, P., Adams, J., Curnoe, D., Maslin, M., 2010. Geochronology and palaeoenvironments of the South African early hominin bearing sites. *Am. J. Phys. Anthr.* 143, 640–646.
- Herries, A.I.R., Kappen, P., Kegley, A., Paterson, D., Howard, D.L., de Jonge, M.D., Potze, S., Adams, J.W., 2014. Palaeomagnetic and synchrotron analysis of >1.95 Ma fossil bearing palaeokarst at Haasgat, Gauteng. *S. Afr. J. Sci.* 110, 1–12.
- Herries, A.I.R., Pickering, R., Adams, J.W., Curnoe, D., Warr, G., Latham, A.G., Shaw, J., 2013. A multi-disciplinary perspective on the age of *Australopithecus* in southern Africa. In: Reed, K.E., Fleagle, J.G., Leakey, R. (Eds.), Paleobiology of *Australopithecus*: Vertebrate Paleobiology and Paleoanthropology Series, pp. 21–40.
- Herries, A.I.R., Shaw, J., 2011. Palaeomagnetic analysis of the Sterkfontein palaeocave deposits; age implications for the hominin fossils and stone tool industries. *J. Hum. Evol.* 60, 523–539.
- Joannes-Boyau, R., 2013. Detailed protocol for accurate non-destructive direct dating of human remains. *Geochronometria* 40, 322–333.
- Joannes-Boyau, R., Grün, R., 2011. A comprehensive model for CO<sub>2</sub>– radicals in fossil tooth enamel: implications for ESR dating. *Quat. Geochronol.* 6, 82–97.
- Joannes-Boyau, R., Duval, M., Bodin, T., 2018. MCDoseE 2.0 a New Markov Chain Monte Carlo Program for ESR Dose Response Curve Fitting and Dose Evaluation Quaternary Geochronology, vol. 44, pp. 13–22.
- Johnson, J.E., Webb, S.M., Ma, C., Fischer, W., 2016. Manganese mineralogy and diagenesis in the sedimentary rock record. *Geochimica Cosmochimica Acta* 173, 210–231.
- Karkanas, P., Goldberg, P., 2007. Micromorphology of sediments: deciphering archaeological context. *Isr. J. Earth Sci.* 56, 63–71.
- Keyser, A.W., 2000. The Drimolen skull: the most complete australopithecine cranium and mandible to date. *South Afr. J. Sci.* 96, 189–193.
- Keyser, A.W., Menter, C.G., Moggi-Cecchi, J., Pickering, T.R., Berger, L.R., 2000. Drimolen: a new hominid-bearing site in Gauteng, South Africa. *South Afr. J. Sci.* 96, 193–197.
- Keyser, A.W., Martini, J.E.J., 1991. Haasgat, a new Plio-Pleistocene fossil locality. *Palaeoecol. Afr.* 21, 119–129.
- Kramers, J.D., Dirks, P.H.G.M., 2017. The age of fossil StW573 ('Little Foot'): reply to comments by Stratford et al. (2017). *South Afr. J. Sci.* 113 (7–8), 1–3. <https://doi.org/10.17159/sajs.2017/a0222>.
- Kramers, J.D., Dirks, P.H.G.M., 2017. The age of fossil StW573 ('Little Foot'): an alternative interpretation of 26Al/10Be burial data. *South Afr. J. Sci.* 113 (3–4), 1–8. <https://doi.org/10.17159/sajs.2017/20160085>.
- Kuhn, B., Herries, A.I.R., Price, G., Baker, S., Hopley, P., Menter, C., Caruana, M., 2016. Renewed investigations at taung; 90 years after *Australopithecus africanus*. *Palaeontol. Afr.* 51, 10–26.
- Lacruz, R.S., Turner, A., Berger, L.R., 2006. New *Dinofelis* (carnivora: machairodontinae) remains from Sterkfontein Valley sites and a taxonomic revision of the genus in southern Africa. *Ann. Transvaal Mus.* 43, 89–106.
- Lascu, I., Harrison, R.J., Li, Y., Muraszko, J.R., Channell, J.E.T., Piotrowski, A.M., Hodell, D.A., 2015. Magnetic unmixing of first-order reversal curve diagrams using principal component analysis. *Geochem. Geophys. Geosystems* 16, 2900–2915. <https://doi.org/10.1002/2015GC005909>.
- Latham, A.G., Herries, A.I.R., Kuykendall, K., 2003. The formation and sedimentary infilling of the Limeworks Cave, Makapansgat, South Africa. *Palaeontol. Afr.* 39, 69–82.
- Latham, A.G., Herries, A., Quinney, P., Sinclair, A., Kuykendall, K., 1999. The Makapansgat australopithecine site from a speleological perspective. In: Pollard, A.M. (Ed.), Geoarchaeology: Exploration, Environments, Resources, vol. 165. Royal Geological Society, London. Special Publications, pp. 61–77.
- Leece, A., Kegley, A., Lacruz, R., Herries, A.I.R., Hemingway, J., Kgasi, L., Potze, S., Adams, J.W., 2016. The first hominin from the early Pleistocene paleocave of Haasgat, South Africa. *PeerJ* 4, e2024. DOI 10.7717/peerj.2024.
- Lui, Q., Yu, Y., Torrent, J., Roberts, A.P., Pan, Y., Zhu, R., 2006. Characteristic low-temperature magnetic properties of aluminous goethite [ $\alpha$ -(Fe, Al)OOH]. *J. Geophys. Res.* 111, B12S34. <https://doi.org/10.1029/2006B004560>.
- Martini, J., Kavalieris, I., 1976. The karst of Transvaal (South Africa). *Int. J. Speleology* 8, 1.
- Maxbauer, D.P., Feinberg, J.M., Fox, D., 2016. MAX UnMix: a web application for unmixing magnetic coercivity distributions. *Comput. Geosciences* 95, 140–145.
- Menter, C.G., Kuykendall, K.L., Keyser, A.W., Conroy, G.C., 1999. First record of hominid teeth from the Plio-Pleistocene site of Gondolin, South Africa. *J. Hum. Evol.* 37, 299–307.
- Moggi-Cecchi, J., Menter, C.G., Boccone, S., Keyser, A., 2010. Early hominin dental remains from the Plio-Pleistocene site of Drimolen, South Africa. *J. Hum. Evol.* 58, 374–405.
- Moskowitz, B.M., Jackson, M., Kissel, C., 1998. Low temperature magnetic behaviour of titanomagnetites. *Earth Planet. Sci. Lett.* 157, 141–149.
- Neal, A., 2004. Ground-penetrating radar and its use in sedimentology: principles, problems and progress. *Earth-Science Rev.* 66 (3–4), 261–330.
- Ogg, J.G., 2012. Geomagnetic polarity Timescale. In: Gradstein, F.M., Ogg, J.G., Schmitz, M. (Eds.), The Geologic Time Scale. Elsevier, Boston, pp. 85–113.
- O'Regan, H.J., Menter, C.G., 2009. Carnivora from the plio-pleistocene hominin site of drimolen, Gauteng, South Africa. *Geobios* 42, 329–350.
- Özdemir, Ö., Dunlop, D., Moskowitz, B.M., 1993. The effect of oxidation on the Verway transition in magnetite. *Geophys. Res. Lett.* 20, 1671–1674.
- Partridge, T.C., 2000. Hominid-bearing cave and tufa deposits. In: Partridge, T.C., Maud, R.R. (Eds.), The Cenozoic of Southern Africa. Oxford University Press, Oxford, pp. 100–125.
- Partridge, T.C., 1978. Re-appraisal of lithostratigraphy of Sterkfontein hominid site. *Nature* 275, 282–287.
- Partridge, T.C., 1979. Re-appraisal of lithostratigraphy of Makapansgat Limeworks hominid site. *Nature* 279, 484–488.
- Partridge, T., Brink, A., 1967. Gravels and terraces of the lower Vaal River basin.

- South Africangeogr. J. 49, 21–38.
- Partridge, T.C., Granger, D.E., Caffee, M.W., Clarke, R.J., 2003. Lower Pliocene hominid remains from Sterkfontein. *Science* 300, 607–612.
- Pickering, R., Kramers, J., Hancox, J., de Ruiter, D., Woodhead, J., 2011a. Contemporary flowstone development links early hominin bearing cave deposits in South Africa. *Earth Planet. Sci. Letts* 306, 23–32.
- Pickering, R., Dirks, P.H.G.M., Jinnah, Z., de Ruiter, D.J., Churchill, S.E., Herries, A.I.R., Woodhead, J.D., Hellstrom, J.C., Berger, L.R., 2011b. Australopithecus sediba at 1.977 Ma and implications for the origins of Genus Homo. *Science* 333, 1421–1423.
- Pickering, R., Kramers, J.D., 2010. Re-appraisal of the stratigraphy and determination of new U-Pb dates for the Sterkfontein hominin site, South Africa. *J. Hum. Evol.* 59, 70–86.
- Pickering, R., Kramers, J.D., Partridge, T., Kodolanyi, J., Pettke, T., 2010. U–Pb dating of calcite–aragonite layers in speleothems from hominin sites in South Africa by MC-ICP-MS. *Quat. Geochronol.* 5, 544–558.
- Pickering, R., Hancox, P.J., Lee-Thorp, J.A., Grün, R., Mortimer, G.E., McCulloch, M., Berger, L.R., 2007. Stratigraphy, U-series chronology and palaeoenvironments at Gladysvale Cave: insights into the climatic control of South African hominin bearing caves, South Africa. *J. Hum. Evol.* 53, 602–619.
- Pueyo Anchuela, Ó., Casas-Sainz, A.M., Soriano, M.A., Pocovi-Juan, A., 2010. A geophysical survey routine for the detection of doline areas in the surroundings of Zaragoza (NE Spain). *Eng. Geol.* 114 (3–4), 382–396.
- Rapp, G.R., Hill, C.L., 2006. *Geoarchaeology: the Earth-science Approach to Archaeological Interpretation*. Yale University Press.
- Reis Jr., J.A.d., de Castro, D.L., de Jesus, T.E.S., Filho, F.P.L., 2014. Characterization of collapsed paleocave systems using GPR attributes. *J. Appl. Geophys.* 103, 43–56.
- Reynolds, S.C., Clarke, R.J., Kuman, K.A., 2007. The view from the Lincoln Cave: mid to late-Pleistocene fossil deposits from Sterkfontein hominid site, South Africa. *J. Hum. Evol.* 53, 260e271.
- Roberts, A.P., Pike, C.R., Verosub, K.L., 2000. First-order reversal curve diagrams: a new tool for characterizing the magnetic properties of natural samples. *J. Geophys. Res. Solid Earth* 105, 461–475.
- Roberts, D., Matthews, T., Herries, A.I.R., Boultter, C., Scott, L., Dondo, C., Ntembi, P., Browning, C., Smith, R., Haarhoff, P., 2011. Regional and global palaeoenvironmental and sea level context of the late cenozoic Langebaanweg (LBW) palaeontological site: west coast of South Africa. *Earth Sci. Revs* 106, 191–214.
- Rodriguez, V., Gutierrez, A., Green, A.G., Carbonel, D., Horstmeyer, H., Schmelzbach, C., 2014. Characterizing sagging and collapse sinkholes in a mantled karst by means of ground penetrating radar (GPR). *Environ. Eng. Geoscience* 20 (2), 109–132.
- Rovinsky, D.S., Herries, A.I.R., Menter, C., Adams, J.W., 2015. First description of in situ primate and faunal remains from the Plio-Pleistocene Drimolen Makondo palaeocave infill, Gauteng, South Africa. *Palaeontol. Electron.* 18(2.34A): 1–21.
- Singer, B.S., 2014. A Quaternary geomagnetic instability time scale. *Quat. Geochron* 21, 29–52.
- Stein, J.K., 2001. A review of site formation processes and their relevance to geoarchaeology. In: Goldberg, P., Holliday, V.T., Ferring, C.R. (Eds.), *Earth Sciences and Archaeology*. Kluwer Academic/Plenum Publishers, New York.
- Stoops, G., 2003. *Guidelines for Analysis and Description of Soil and Regolith Thin Sections*. Soil Science Society of America, Madison, Wisconsin, USA.
- Stratford, D.J., Bruxelles, L., Clarke, R.J., Kuman, K., 2012. New stratigraphic interpretations of the fossil and artefact-bearing deposits of the Name Chamber, Sterkfontein. *S. Afr. Afr. Archaeol. Bull.* 67, 159–167.
- Stratford, D.J., Grab, S., Pickering, T.R., 2014. The stratigraphy and formation history of fossil- and artefact-bearing sediments in the Milner Hall, Sterkfontein Cave, South Africa: new interpretations and implications for palaeoanthropology and archaeology. *J. Afr. Earth Sci.* 96, 155–167.
- Turekian, K.K., Wedepohl, K.H., 1961. Distribution of the elements in some major units of the earth's crust. *Geol. Soc. Am. Bull.* 72, 175–192.
- Walker, J., Cliff, R.A., Latham, A.G., 2006. U–Pb isotopic age of the StW 573 hominid from Sterkfontein, South Africa. *Science* 314, 1592–1594.
- Waters, M.R., 1996. *Principles of Geoarchaeology: a North American Perspective*. University of Arizona Press.
- Waters, M.R., Kuehn, D.D., 1996. The geoarchaeology of place: the effect of geological processes on the preservation and interpretation of the archaeological record. *Am. Antiqu.* 483–497.
- Werdelin, L., Peigne, S., 2010. Carnivora. In: Werdelin, L., Sanders, W. (Eds.), *Cenozoic Mammals of Africa*. University of California Press, Berkeley, pp. 603–658.
- Werdelin, L., Ewer, M.E., 2001. A revision of the genus *Dinofelis* (mammalia, felidae). *Zoological J. Linn. Soc.* 132, 147–258.
- Woodhead, J.D., Pickering, R., 2012. Beyond 500 ka: progress and prospects in the U–Pb chronology of speleothems, and their application to studies in palaeoclimate, human evolution, biodiversity and tectonics. *Chem. Geol.* 322–323, 290–299.
- Woodhead, J., Hellstrom, J., Maas, R., Drysdale, R., Zanchetta, G., Devine, P., 2006. U–Pb geochronology of speleothems by MC-ICPMS. *Quat. Geochronol.* 1, 208–221.
- Woodhead, J., Hellstrom, J., Pickering, R., Drysdale, R., Paul, B., Bajo, P., 2012. U and Pb variability in older speleothems and strategies for their chronology. *Quat. Geochronol.* 14, 105–113.